Annu. Rev. Fluid Mech. 2004. 36:413–55
doi: 10.1146/annurev.fluid.36.050802.122128

VORTEX-INDUCED VIBRATIONS

C.H.K. Williamson[1] and R. Govardhan[2]
[1]*Mechanical and Aerospace Engineering, Upson Hall, Cornell University, Ithaca, New York 14853; email: cw26@cornell.edu*
[2]*Mechanical Engineering Department, Indian Institute of Science, Bangalore, India; email: raghu@mecheng.iisc.ernet.in*

Key Words resonance, synchronization, lock-in, wake modes, vortex dynamics

■ **Abstract** This review summarizes fundamental results and discoveries concerning vortex-induced vibration (VIV), that have been made over the last two decades, many of which are related to the push to explore very low mass and damping, and to new computational and experimental techniques that were hitherto not available. We bring together new concepts and phenomena generic to VIV systems, and pay special attention to the vortex dynamics and energy transfer that give rise to modes of vibration, the importance of mass and damping, the concept of a critical mass, the relationship between force and vorticity, and the concept of "effective elasticity," among other points. We present new vortex wake modes, generally in the framework of a map of vortex modes compiled from forced vibration studies, some of which cause free vibration. Some discussion focuses on topics of current debate, such as the decomposition of force, the relevance of the paradigm flow of an elastically mounted cylinder to more complex systems, and the relationship between forced and free vibration.

1. INTRODUCTION

Vortex-induced vibration (VIV) of structures is of practical interest to many fields of engineering. For example, it can cause vibrations in heat exchanger tubes; it influences the dynamics of riser tubes bringing oil from the seabed to the surface; it is important to the design of civil engineering structures such as bridges and chimney stacks, as well as to the design of marine and land vehicles; and it can cause large-amplitude vibrations of tethered structures in the ocean. These are a few examples out of a large number of problems where VIV is important. The practical significance of VIV has led to a large number of fundamental studies, many of which are discussed in the comprehensive reviews of Sarpkaya (1979), Griffin & Ramberg (1982), Bearman (1984), Parkinson (1989); in a book chapter by Anagnostopoulos (2002); and in books by Blevins (1990), Naudascher & Rockwell (1994), and Sumer & Fredsøe (1997). Here we focus on the more recent accomplishments of researchers, especially within the last decade. One stimulus for a resurgence of interest in VIV came from the Ocean Engineering Division of

the U.S. Office of Naval Research, which mounted a University Research Initiative and brought together many international researchers to work on common ground. This also led to focused conferences, supported by the ONR, IUTAM, and ASME, and other international bodies, on this topic, namely the series *Bluff Body Wakes and Vortex-Induced Vibrations* (*BBVIV*), which has been held in Washington, D.C. (1998); Marseille, France (2000); and Port Douglas, Queensland (2002).

In this review, we are concerned principally with the oscillations of an elastically mounted rigid cylinder; with forced vibrations of such structures; with bodies in two degrees of freedom; with the dynamics of cantilevers, pivoted cylinders, cables, and tethered bodies. As a paradigm for such VIV systems, we shall consider here an elastically mounted cylinder restrained to move transverse to the flow, as Figure 1*a* shows. As the flow speed (U) increases, a condition is reached when the vortex formation frequency (f_V) is close enough to the body's natural frequency (f_N) such that the unsteady pressures from the wake vortices induce the body to respond. Certain wake patterns can be induced by body motion, such as the 2S mode (2 single vortices per cycle, like the classic Karman street) and the 2P mode (comprising 2 vortex pairs formed in each cycle of body motion), following the terminology introduced in Williamson & Roshko (1988). Interestingly, a forced vibration can also lead to other vortex modes including a P + S mode, which is not able to excite a body into free vibration. In essence, a nominally periodic vibration ensues if the energy transfer, or work done by the fluid on the body, over a cycle is positive. This net energy transfer is influenced significantly by the phase of induced side force relative to body motion, which in turn is associated with the timing of the vortex dynamics. The problem of VIV is therefore a fascinating feedback between body motion and vortex motion. In this review we present not only response phenomena, but also the important vortex dynamics modes leading to the response.

Even in the simple case of the elastically mounted cylinder many fundamental questions exist that are outstanding, for example: (*a*) What is the maximum possible amplitude attainable for a cylinder undergoing VIV, for conditions of extremely small mass and damping? (*b*) Under what conditions does the classically employed mass-damping parameter collapse peak-amplitude data? What is the functional shape for a plot of peak amplitude versus mass-damping? (*c*) What modes of structural response exist, and how does the system jump between the different modes? (*d*) What vortex dynamics give rise to the different body response modes? (*e*) What generic features can be discovered that are applicable to all VIV systems? To what extent are the enormous number of studies for bodies restricted to motion transverse to the flow, relevant to other, more complex VIV systems? (*f*) Because almost all of the studies of VIVs are at low and moderate Reynolds numbers, how do these results carry across to high Reynolds numbers?

This review brings together for the first time a number of new phenomena, many of which are related to the above questions. One fascinating phenomenon, which highlights the potential for new techniques since the previous review by Bearman (1984) in *Annual Review of Fluid Mechanics*, comes from low-Reynolds-number

(Re = 100) computations undertaken by Tony Leonard, Doug Shiels, and Anatol Roshko at Caltech (Shiels et al. 2001), and is seen in Figure 1. The wake is essentially a Karman vortex street, but is actually generated by a body that has no mass, no spring, and no damping! At every instant in time, the transverse ideal added mass force is exactly balanced by the vortex force. This phenomenon is but one in a whole set of new results made possible by accurate use of new methods. Computational studies are used to attack two- and three-dimensional flows, as well as to compute higher-Reynolds-number flows, bodies of long aspect ratio, and flexible structures. On the other hand, experimentalists now extensively utilize the highly effective Particle-Image Velocimetry (PIV) technique to determine vorticity.

Here we introduce an equation of motion generally used to represent VIV of a cylinder oscillating in the transverse Y direction (normal to the flow) as follows:

$$m\ddot{y} + c\dot{y} + ky = F, \tag{1}$$

where m = structural mass, c = structural damping, k = spring constant, and F = fluid force in the transverse direction. In the regime where the body oscillation frequency is synchronized with the periodic vortex wake mode (or periodic fluid force), a good approximation to the force and the response is given by

$$\mathrm{F(t)} = \mathrm{F_o}\sin(\omega t + \phi) \tag{2}$$

$$\mathrm{y(t)} = \mathrm{y_o}\sin(\omega \mathrm{t}), \tag{3}$$

where $\omega = 2\pi \mathrm{f}$ and f = body oscillation frequency. The response amplitude and frequency may be derived in a straightforward manner from Equations 1–3, as done by several previous investigators. Here we formulate the equations in terms of a chosen set of nondimensional parameters, as in Khalak & Williamson (1999):

$$\mathrm{A}^* = \frac{1}{4\pi^3}\frac{C_Y \sin\phi.}{(m^* + C_A)\,\varsigma}\left(\frac{U^*}{f^*}\right)^2 f^* \tag{4}$$

$$\mathrm{f}^* = \sqrt{\frac{m^* + C_A}{m^* + C_{EA}}}, \tag{5}$$

where $\mathrm{C_A}$ is the potential added mass coefficient (taking the value 1.0), and $\mathrm{C_{EA}}$ is an "effective" added mass coefficient that includes an apparent effect due to the total transverse fluid force in-phase with the body acceleration ($\mathrm{C_Y}\cos\phi$):

$$\mathrm{C_{EA}} = \frac{1}{2\pi^3}\frac{C_Y \cos\phi}{A^*}\left(\frac{U^*}{f^*}\right)^2. \tag{6}$$

Quantities in the above equations are defined in the Appendix. Animated debate often surrounds the definition of added mass ($\mathrm{C_{EA}}$) in these problems. Of course, it is not a true added mass, because it has a significant force component due to the vorticity dynamics. Note that the amplitude A^* in Equation 4 is proportional to the

transverse force component that is in-phase with the body velocity ($C_Y \sin\phi$), and, for small mass and damping, the precise value of the phase angle ϕ has a large effect on the response amplitude.

Feng (1968) contributed some important classic measurements of response and pressure for an elastically mounted cylinder. Figure 2*a* presents his minimum damping case, and it is apparent that there are two amplitude branches, namely the "initial" branch and the "lower" branch (in the terminology of Khalak & Williamson 1996), with a hysteretic transition between branches. The mass ratio (or relative density) is very large because the experiments were conducted in air ($m^* \sim 250$). Much of the new work we review in the following sections comes from the push to explore much smaller mass and damping, generally using water as the fluid medium. Regarding the frequency response, the classical definition of lock-in or synchronization is often perceived as the regime where the frequency of oscillation (f), as well as the vortex formation frequency (f_V), are close to the natural frequency (f_N) of the structure throughout the regime of large-amplitude vibration, so that $f^* = f/f_N \sim 1$ in Figure 2*b*. However, recent studies (in Sections 2 and 3) show a dramatic departure from this classical result; bodies can conceivably vibrate with large amplitude, at hundreds of times the natural frequency!

Feng also noted that the jump in response amplitude was reflected by a significant jump in the phase of the pressure fluctuations relative to body motion. One might suspect that a jump in phase angle (between transverse force and displacement) through resonance, as shown in Figure 2*c*, will be matched by a switch in the timing of vortex shedding. Zdravkovich (1982) showed this for the first time using visualisations from previous studies. An excellent demonstration of this timing switch comes from the comprehensive forced vibration study of Ongoren & Rockwell (1988a), shown in Figure 3*a*, where the switch in timing of vortex formation is evident as the body's frequency is increased through a critical value (roughly $f/f_V \sim 1.05$). Gu, Chyu & Rockwell (1994) confirmed this from forced vibrations at small $A^* = 0.2$, in the groundbreaking first study of this problem using PIV. This phenomenon has also been found in the simulations of Meneghini & Bearman (1993, 1995), Lu & Dalton (1996), Blackburn & Henderson (1999), Anagnostopoulos (2000a,b), Guilmineau & Queutey (2002), and further experiments by Krishnamoorthy et al. (2001).

It is important to ask what the relationship is between the maximum response amplitude and the system mass and damping. Generally, this information has been

Figure 2 Free vibration of an elastically mounted cylinder at high mass ratios. In (*a*), we compare the classical response amplitudes of Feng (1968) (*triangle symbols*), with Brika & Laneville (1993) (*open symbols*), both at the same ($m^*\zeta$) in air. (*b*) and (*c*) show the vibration frequency and phase of the transverse force, as measured in water, but with the same ($m^* + C_A)\zeta \sim 0.251$ as used in the air experiments (Govardhan & Williamson 2000). Brika & Laneville's smoke visualizations (*d*) showed for the first time that the response branches correspond with the 2S and 2P modes.

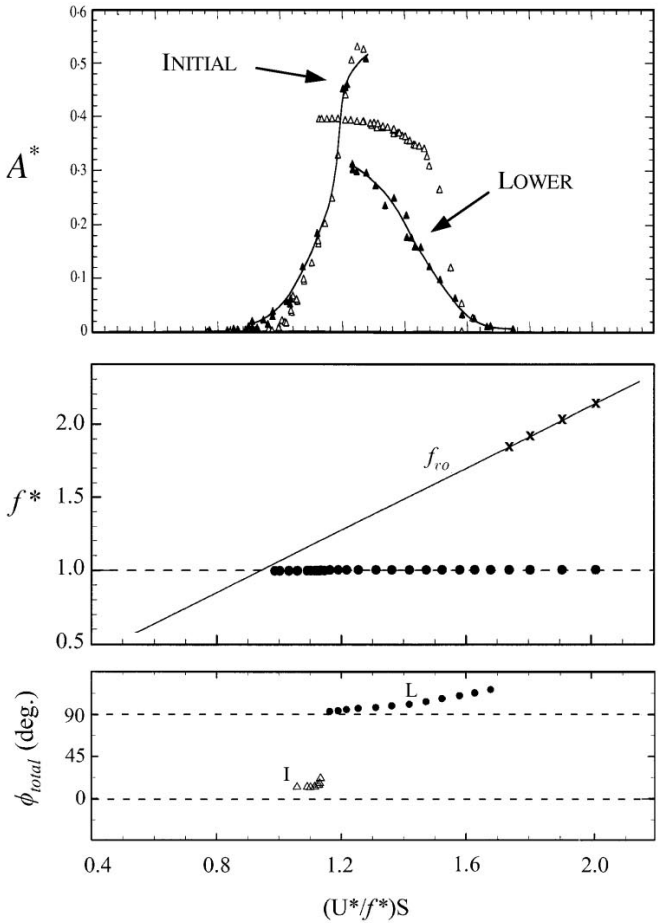

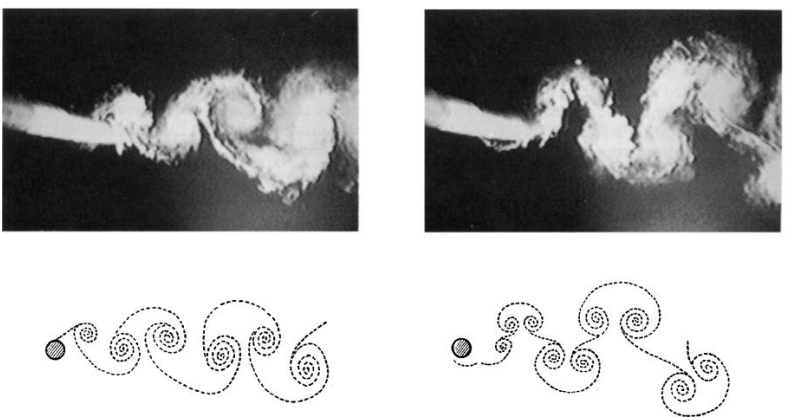

plotted as A^*_{max} versus a parameter, S_G, proportional to the product of mass and damping, following the first comprehensive compilation of existing data by Griffin and coworkers in the 1970s, and labeled for convenience as the "Griffin plot" by Khalak & Williamson (1999). Figure 3*c* shows one of Griffin's (1980) original plots, illustrating the characteristic shape whereby the amplitude reaches some limiting value as S_G (reduced damping) becomes small. The logic in choosing a combined mass-damping parameter comes from Equation 4 for A^*. For example, Bearman (1984) demonstrated that for large mass ratios ($m^* \gg 1$), the actual cylinder oscillation frequency (f) at resonance will be close to the vortex shedding frequency for the static cylinder (f_V), and also close to the system natural frequency (f_N), i.e., $f \approx f_V \approx f_N$, and thus $f^* \approx 1.0$ (see Equation 5 for large m^*). Thus, at resonance, the parameter $(U^*/f^*) = (U/fD) \approx (U/f_V\, D) = 1/S$, where S is the Strouhal number of the static cylinder, suggesting a resonance at the normalized velocity, $U^* \approx 5$–6. Therefore, the assumption is often made that both (U^*/f^*) and f^* are constants, under resonance conditions, giving (from Equation 4)

$$A^*_{max} \propto \frac{C_Y \sin\phi.}{(m^* + C_A)\varsigma}. \tag{7}$$

As Khalak & Williamson (1999) discussed, if (U^*/f^*) is assumed constant, then the excitation ($C_Y \sin\phi$) is a function of $\{A^*\}$ only. Therefore, under these assumptions, A^*_{max} is a function only of the product of mass and damping $(m^* + C_A)\zeta$. We stress that Equation 7 depends on the earlier assumptions remaining reasonable, namely that $f^* \approx 1.0$, which is not self-evident. The Griffin plot has become an integral part of the offshore design codes (for example, *Det Norske Veritas* codes), and so it is important to determine it accurately. As discussed in Section 4, a final accurate definition of this important plot is surprisingly not yet available.

Aside from studies of elastically mounted structures, one approach to an understanding and possible prediction of vibrations has been to undertake forced vibrations of a structure. A central contribution of Sarpkaya to VIV has been his well-known and much-referenced data set of transverse force coefficients for controlled sinusoidal vibration of a cylinder transverse to a free stream. Sarpkaya (1977, 1978) expressed the transverse force as

$$C_Y = C_{my} \sin\omega t - C_{dy} \cos\omega t, \tag{8}$$

where C_{my} and C_{dy} are the inertia (in-phase) and drag (out-of-phase) force coefficients of the transverse force coefficient C_Y. An example set of data, at constant amplitude ($A^* = 0.5$) and for varying normalized velocity, $V_R St$, which is equivalent to $(U^*/f^*)S$, is included in Figure 3*d* (from Sarpkaya 1995), where he included more recent data from Moe & Wu (1990) and Gopalkrishnan (1993). We note that the agreement between these newer data sets and his own classical data is remarkable despite the different experimental conditions. Further discussion of forced vibrations will be presented in Section 5.

Williamson & Roshko (1988) studied the vortex wake patterns for a cylinder, translating in a sinusoidal trajectory, over a wide variation of amplitudes (A/D up

to 5.0) and wavelengths (λ/D up to 15.0). They defined a whole set of different regimes for vortex wake modes, using controlled vibrations, in the plane of $\{\lambda/D, A/D\}$, where a descriptive terminology for each mode was introduced. Each periodic vortex wake pattern comprises single vortices (S) and vortex pairs (P), giving patterns such as the 2S, 2P, and P + S modes, which are the principal modes near the fundamental lock-in region in Figure 4. Visualization of the 2P mode is clearly presented in this figure also. Williamson & Roshko (1988) described other patterns, such as those formed by coalescence of vortices, or from more vortices per cycle (e.g., the "2P + 2S," representing a one-third-subharmonic mode).

The 2P and P + S modes have been found in controlled vibration studies in-line with the flow (Griffin & Ramberg 1976, Ongoren & Rockwell 1988b). The P + S mode was also found in Griffin & Ramberg's (1974) well-known smoke visualizations for transverse motions (see also Zdera et al. 1995). The significance of these modes from controlled vibration is that they provide a map of regimes within which we observe certain branches of free vibration. One deduction from the Williamson & Roshko study was that the jump in the phase ϕ of the transverse force in Bishop & Hassan's (1964) classical forced vibration paper, and also the jump in phase measured in Feng's (1968) free-vibration experiments, were caused by the changeover of mode from the 2S to the 2P mode. This has since been confirmed in a number of free-vibration studies, and we address this in Section 2. Such vortex modes occur for bodies in one or two degrees of freedom, for pivoted rods, cantilevers, oscillating cones, and other bodies. Response data from all of these studies have been correlated with the map of regimes described above.

2. FREE VIBRATION OF A CYLINDER

Brika & Laneville (1993, 1995) were the first to show evidence of the 2P vortex wake mode from free vibration, using a vibrating cable in a wind tunnel. They stated that "the 2S and 2P modes can be clearly recognized, and the earlier explanation by Williamson & Roshko (1988) for the hysteresis loop in terms of a change in wake vortex patterns is confirmed." Figure 2*d* shows their smoke visualization of these modes. They found a clear correspondence of the 2S mode with the initial branch of response, and the 2P mode with the lower branch.

Phenomena at low mass ratios and low mass-damping are distinct from those mentioned above. A direct comparison is made between the response in water ($m^* = 2.4$) (from Khalak & Williamson 1997b), with the largest response plot of Feng conducted in air (Figure 5). The lighter body has a value of ($m^*\zeta$), around 3% of Feng's value, yielding a much higher peak amplitude. The extent of U^* over which there is significant response is four times larger than that found by Feng. (The widening of the synchronization regime for decreasing mass is an effect which was shown by Griffin & Ramberg 1982). Although these are trends that might be expected, the character of the response for low mass-damping is also distinct. The low-($m^*\zeta$) type of response is characterized by not only the initial branch and the

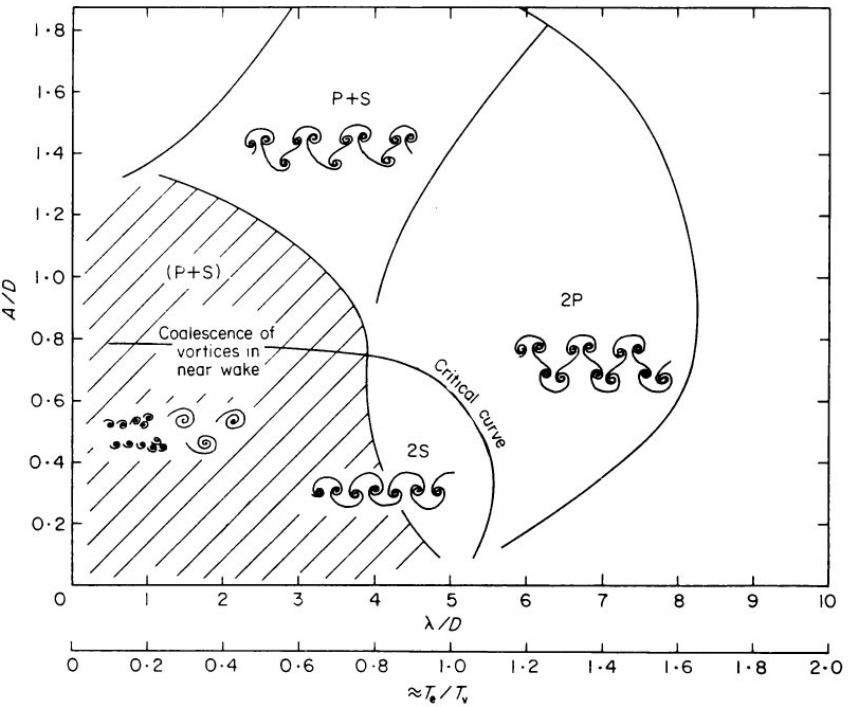

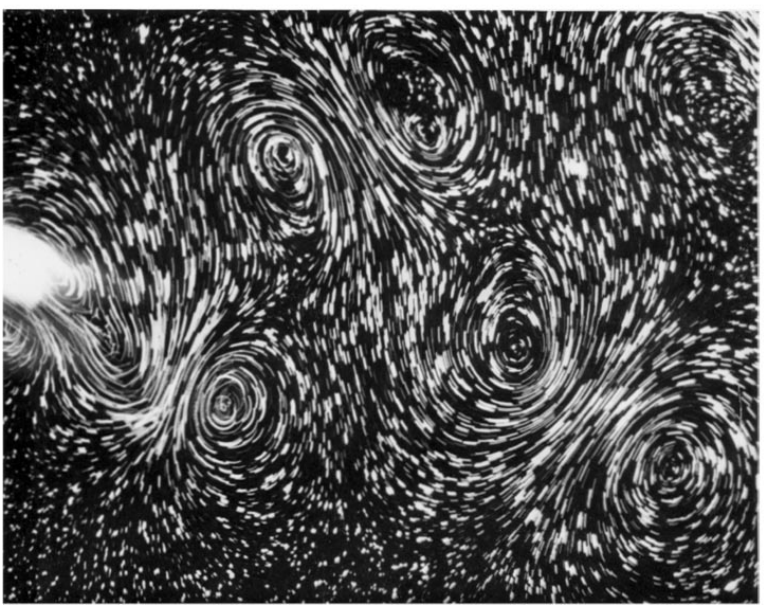

lower branch, but also by the new appearance between the other two branches of a much higher "upper response branch." Khalak & Williamson (1996; 1997a,b; 1999) showed the existence of these three distinct branches, and using the Hilbert Transform to find instantaneous phase, force, and amplitude, they showed that the transition between the Initial $\Leftrightarrow$ Upper branches is hysteretic, while the Upper $\Leftrightarrow$ Lower transition involves instead an intermittent switching. On the other hand, in Figure 2, for high mass-damping, it is well known that Feng (1968) found a hysteresis between the initial and lower branches.

The phenomenon of lock-in, or synchronization (see Blevins 1990, Sumer & Fredsøe 1997), traditionally means that the ratio $f^* = f/f_N$ remains close to unity, as seen in Figure 2 for high mass ratio. However, for light bodies in water, in this case for $m^* = 2.4$ in Figure 5, the body oscillates at a distinctly higher frequency ($f^* = 1.4$). Experimentally, the departure of f^* from unity, through the lock-in regime, was shown by Moe & Wu (1990), and more recently was reported in Khalak & Williamson (1997b, 1999) and in Gharib et al. (1998). Therefore, one might define synchronization as the matching of the frequency of the periodic wake vortex mode with the body oscillation frequency. Correspondingly, the force frequency must match the oscillation frequency, which is the definition of lock-in now used by Sarpkaya (1995).

It is relevant to mention some early experiments of Meier-Windhorst (1939), who measured the response of a very short cylinder section immersed in a shallow "water table" flow, giving a length/diameter of only 1.8. He used end plates, that moved with the body, which were wider than the cylinder length. The fact that his cylinder arrangement moved in an arc results in a contribution to the effective restoring force coming from the drag force, thereby leading to nonlinearities in spring stiffness. As discussed in Naudascher & Rockwell (1994), the "data includes unusual end effects, because of the small depth of his test section." Despite the fact that there are discrepancies of around 100% in amplitude when plotted against recent data in the Griffin plot, the data curves suggest that an upper branch appears for sufficiently low damping.

Donald Rockwell's group at Lehigh University (see Gu et al. 1994) was the first to measure vorticity dynamics using PIV on the problem of controlled cylinder vibration. The first vorticity measurements for free vibrations, by Govardhan & Williamson (2000), confirmed that the initial and lower branches correspond to the 2S and 2P vortex wake modes, and these are illustrated in Figure 6. The upper branch comprises the 2P mode, but the second vortex of each pair (in each half cycle) is much weaker than the first one, as seen in Figure 6*b*. One of the first

Figure 4 The map of regimes for vortex wake modes (Williamson & Roshko 1988), showing principally the 2S, 2P, and P + S mode regimes, which are relevant to the fundamental synchronization regime. The 2P mode, comprising two vortex pairs per half cycle, is visualized clearly below the mode map. Cylinder is towed through fluid in a sinusoidal trajectory to the left.

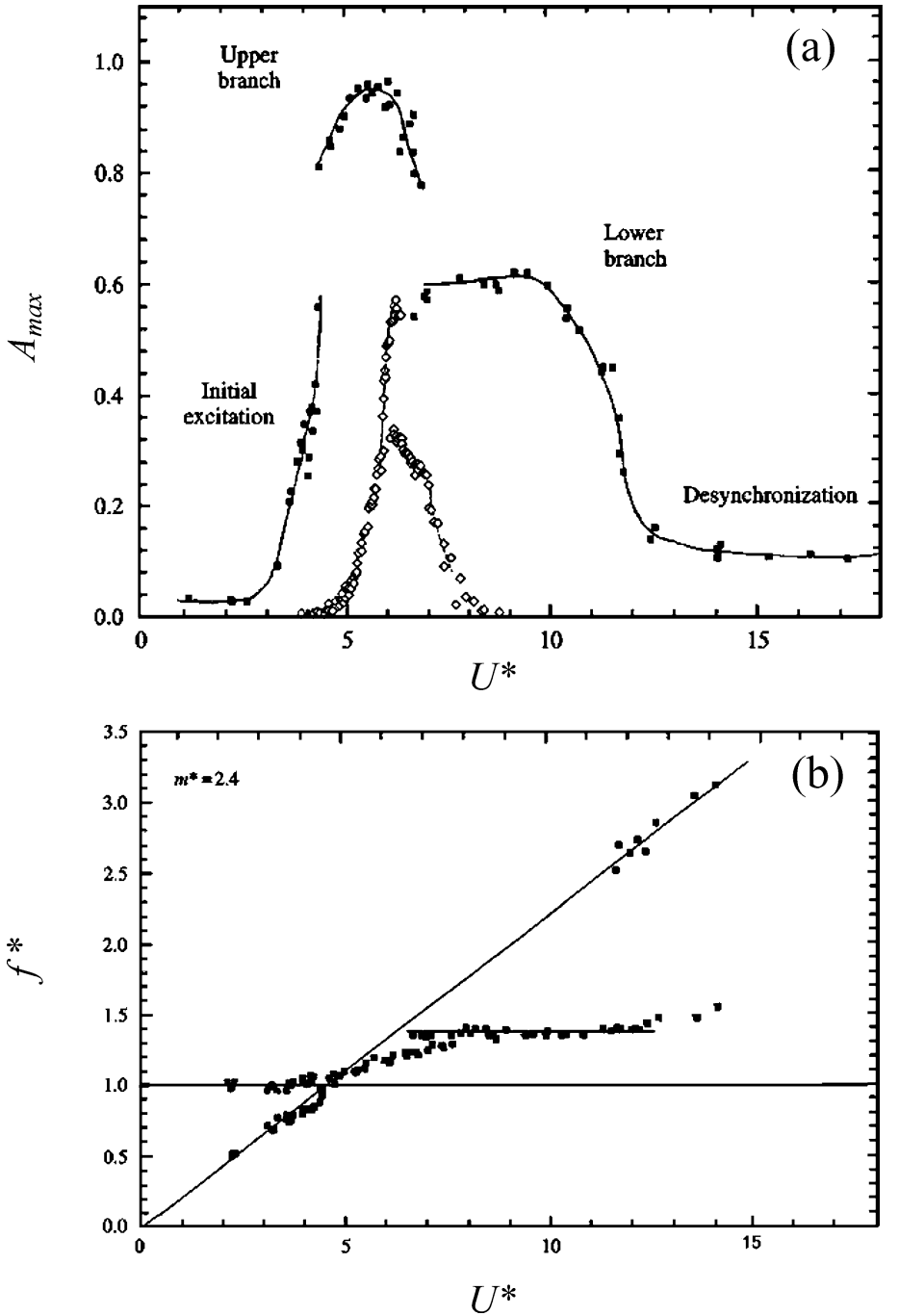

Direct Numerical Simulations (DNS) of the 2P mode, by Blackburn et al. (2001), is included in Figure 6*d*, and represents a direct comparison of vorticity dynamics between numerical and physical experiments.

It is well known that a reduction in mass, for example from $m^* = 8.6$ to 1.2, in Figure 7, leads to a wider synchronization regime, in this case yielding a significant increase of the lock-in regime, which reaches $U^* \approx 17$. The normalized velocity used here, U^*, is the traditional parameter for free-vibration experiments. However, by replotting the data versus the parameter $(U^*/f^*)\,S$, which is equivalent to (f_{vo}/f) (or the inverse of the ratio of actual oscillating frequency to the fixed-body shedding frequency), the data sets collapse very well. Khalak & Williamson (1999) made the first such collapse of free-vibration data and showed that this collapse cannot *a priori* be predicted. An equivalent "true" reduced velocity has been used, not only in the numerical simulations, but also in experiment (Moe & Wu 1990, Hover et al. 1998, Sarpkaya 1995). With the renormalization above, there is a good correspondence between the vortex wake modes of the free response branches with the vortex mode regimes deduced from forced vibration in the Williamson & Roshko map (see Figure 7*b*).

Consider the switch in the timing of vortex shedding described by Zdravkovich (1982) when the amplitude jumps from the initial to lower branch in high mass-damping cases such as Feng (1968). In contrast, for low mass and damping, there are two mode jumps, and it is not immediately clear which one corresponds to the switch in vortex shedding timing. To throw light on this question, Govardhan & Williamson (2000) considered the "total" fluid force, as well as the "vortex" force. The concept of vortex force, or the relationship between impulse of vorticity and fluid momentum, has been used extensively in fluid mechanics (Lamb 1932, Moreau 1953, Batchelor 1967, Saffman 1992). In the present context, Lighthill (1979, 1986) showed that the total fluid force (F_{TOTAL}) can be split into a "potential force" component $F_{POTENTIAL}$, given in this case by the potential added mass force, and a "vortex force" component (F_{VORTEX}) that is due only to the dynamics of all the shed vorticity. The idea of relating force in a qualitative manner to the vortex dynamics was used, for example, in Maull & Milliner (1978) and Williamson (1985), the latter triggered by Lighthill (1979).

In some computational methods, particularly vortex methods, an evaluation of the total fluid force on a body is often made by adding potential and vortex force components. In Govardhan & Williamson's (2000) experimental study, they approached the study of the forces from a different perspective; they set out to deduce what the vortex force is, from direct experimental measurement of the total fluid force. The vortex force F_{VORTEX}, can be simply computed from the total

←

Figure 5 Free vibration at low mass and damping is associated with the existence of an upper branch of high amplitude response, which appears between the initial and lower branches. The frequency of the lower branch is not close to the natural frequency, and is remarkably constant in (*b*). From Khalak & Williamson (1997b). Open symbols in (*a*) show the contrasting high-$m^*\zeta$ response data of Feng (1968).

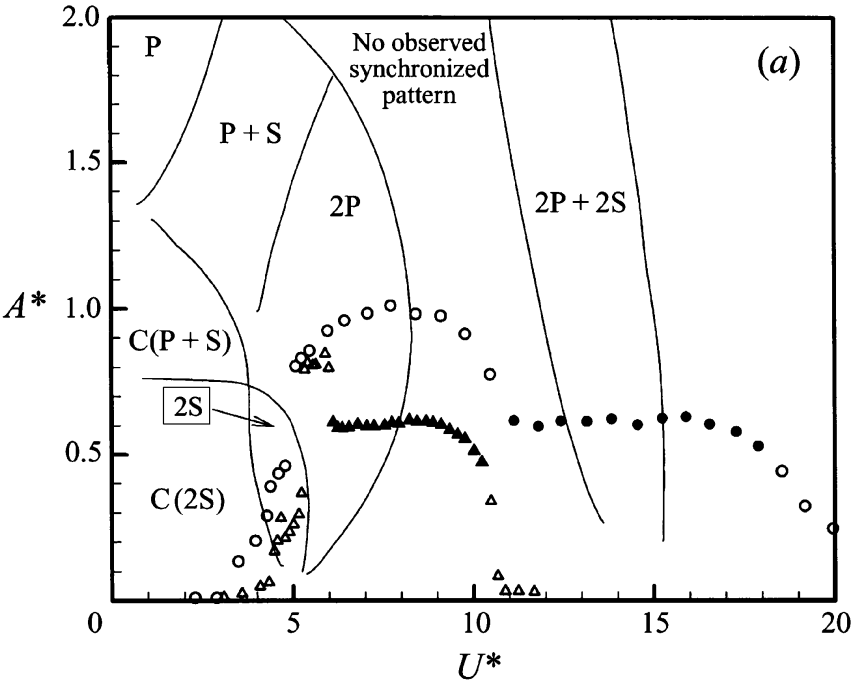

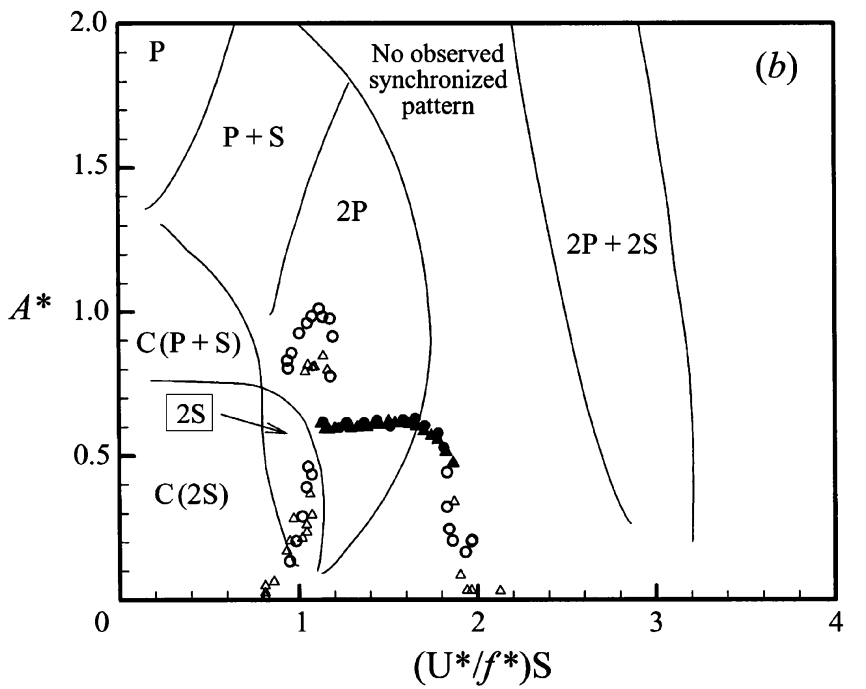

fluid force: $F_{VORTEX}\,(t) = F_{TOTAL}\,(t) - F_{POTENTIAL}\,(t)$, where the potential force is given by $F_{POTENTIAL}\,(t) = -[C_A \cdot m_d \cdot \ddot{y}(t)]$, and where m_d = displaced fluid mass $= (\pi \rho D^2 L/4)$, and C_A is the ideal added mass ($= 1.0$). How can one write the equation of motion in such a manner as to indicate necessarily when a jump in the timing of vortex formation may be found? One can do this by retaining only the vortex force on the right-hand-side of the equation of motion. Govardhan & Williamson thus introduced a "vortex force coefficient" and a "vortex phase," ϕ_{VORTEX}, defined as the phase between vortex force and displacement, writing the equation of motion as:

Equation using "Vortex force":

$$(m + m_A)\ddot{y} + c\dot{y} + ky = F_{VORTEX} \sin(\omega t + \phi_{VORTEX}), \tag{9}$$

whose solution is compared to that from the traditional equation of motion:

Equation using "Total force":

$$m\ddot{y} + c\dot{y} + ky = F_{TOTAL} \sin(\omega t + \phi_{TOTAL}). \tag{10}$$

Absorption of the added mass (m_A) into the total oscillating mass has sometimes been used in texts on fluid-structure interactions (e.g., Blevins 1990, Sumer & Fredsøe 1997), and it is often used in offshore engineering to predict force and dynamics of structures. The new idea in the present context was to define and to evaluate these parameters $\{F_{VORTEX}, \phi_{VORTEX}, F_{TOTAL}, \phi_{TOTAL}\}$ directly from actual experiments. The overview diagram in Figure 8 summarizes how there are two distinctly different jumps between modes for low ($m^*\zeta$). In essence, the transition from initial $\rightarrow$ upper branch is associated with a jump in vortex phase ϕ_{VORTEX}, as the response frequency passes through the value $f = f_{N\ MEDIUM}$ (natural frequency in the fluid medium; for example, water). At this transition there is a switch in the timing of vortex shedding that is associated with the jump from the 2S to the 2P vortex modes. The second transition from upper $\rightarrow$ lower branch corresponds with a jump in total phase ϕ_{TOTAL}, as the response frequency passes through the value $f = f_{N\ VACUUM}$. This transition is *not* associated with a switch in timing of the shedding, in contrast to Zdravkovich's (1982) deductions at high mass-damping.

We briefly return to the important and much-debated question of added mass. As mentioned above, Lighthill (1979, 1986) discussed a formal decomposition of the total fluid force into its potential and vortex force components. As Lighthill

Figure 7 Effect of a mass reduction can dramatically increase the width of the synchronization regime ($m^* = 8.63$ and 1.19) when plotted with velocity (U^*) used traditionally for free vibration. These response data collapse well if one uses the "true" normalized velocity (U^*/f^*)S, yielding a good correspondence between response branches and vortex mode regimes in Williamson & Roshko's (1988) map. From Govardhan & Williamson (2000).

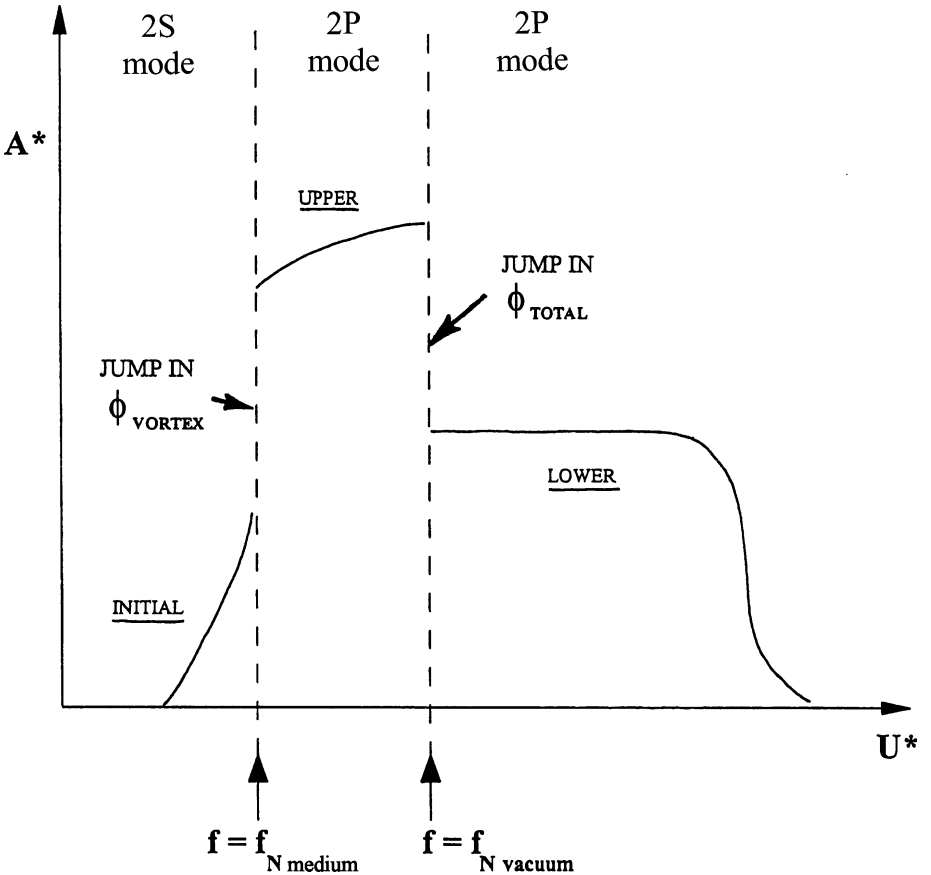

Figure 8 Overview diagram of the low-$m^*\zeta$ type of response, showing the three principal branches, and the corresponding two jump phenomena. This plot shows the jump in vortex phase (ϕ_{VORTEX}) and the jump in total phase (ϕ_{TOTAL}), as the vibration frequency passes through the natural frequency in the fluid medium ($f_{N\text{-}WATER}$), and the natural frequency in vacuum ($f_{N\text{-}VACUUM}$), respectively. From Govardhan & Williamson (2000).

put it, the "additional" vorticity (ω_A), which contributes to the vortex force, refers to the entire vorticity in the flow field minus "part of the distribution of vorticity attached to the boundary in the form of a vortex sheet allowing exactly the tangential velocity (slip) associated with the potential flow." A full knowledge of the vorticity field would yield the vortex force through the concept of vorticity impulse. As Koumoutsakos & Leonard (1995) wrote, the total force on a body (per unit length) is given by

$$F_V = \rho \frac{d}{dt} \int (\boldsymbol{\omega}_A \times \boldsymbol{x})\, dV + \frac{\rho \pi D^2}{4} \frac{dU}{dt}. \tag{11}$$

One of the more recent debates comes from the *BBVIV-3* Conference in Marseille, in June 2000 (see Leweke, Bearman & Williamson 2001), which triggered much-needed clarification. Leonard & Roshko (2001) specifically discussed added mass of an accelerating body, defining it as "the impulse given to the fluid during an incremental change of body velocity, divided by that incremental velocity." They point out that such "properties of the added mass are well known from textbook derivations which are usually obtained for irrotational flow, and so it is not as well known that the resulting definitions are applicable more generally, e.g., in separated flows, such as those that occur in problems of flow-induced vibration. As a result, empirical relations are sometimes introduced into models, unnecessarily." Leonard & Roshko provide a clear proof for the validity of the decomposition of the force in a general viscous flow, which of course includes bluff bodies undergoing VIV.

Sarpkaya (2001) made a contrasting conclusion, stating that "Lighthill's assertion that the viscous drag force and the inviscid inertia force acting on a bluff body immersed in a time-dependent flow operate independently, is not in conformity with the existing exact solutions and experimental facts." Sarpkaya quoted an exact solution given in a famous paper by Stokes (1851) concerning the force F(t) on an oscillating sphere in a viscous fluid, valid for small amplitude. He presented the solution as his proof that "it is impossible to decompose F(t), for the flow under consideration, into an inviscid inertia force and a viscous force." Sarpkaya concluded that such a force decomposition is equally impossible in the case of the transverse forces acting on bluff bodies undergoing VIV.

It is important to note the use of terminology in these problems, particularly where it is used in practice. For example, it is common in offshore engineering to use the expression "added mass" to mean all the fluid force in phase with acceleration (see, for example, Vikestad et al. 2000), which is distinct from the potential added mass.

There have been excellent advances in the methods to measure induced force on a body, employing the concept of vorticity impulse. Two research groups, one at Lehigh University and the other at Caltech, have been pushing forward these techniques, coupled with their development of highly accurate PIV techniques. Lin & Rockwell (1996) found good agreement when comparing the directly measured lift force with the force computed from vorticity, effectively using Equation 11. Because the vorticity remained in the neighborhood of the body, they could take into account all the vorticity. However, in VIV problems, the flow domain is too large to capture fully, and there have therefore been developments to compute the force by measuring the velocity field and its derivatives within a finite control volume surrounding the body, as shown in papers by Unal et al. (1997) and Noca et al. (1997, 1999). Noca et al. (1999) employed a relation that only requires evaluating velocity derivatives on the external control surface. The sophisticated derivations and new relations in these papers are a major step forward, although some problems remain with implementing the methods in practice.

3. EXISTENCE OF A "CRITICAL MASS"

We see from several investigations that, as the structural mass decreases, so the regime of velocity U^* over which there are large-amplitude vibrations increases (see, for example, Figure 7). Anthony Leonard indicated the large extent of such regimes for very low mass ratios, based on results related to numerical simulation, at the ONR Meeting at Brown University (June 1997). We make the deduction here that when mass ratio (m^*) tends to zero, then the extent of the synchronization regime of large-amplitude motion extends to infinity! (We simply deduce this from Equation 5.) However, a more surprising result shows that the synchronization regime becomes infinitely wide, not simply when the mass becomes zero, but when the mass falls below a special critical value whose numerical value depends on the shape of the vibrating body.

The higher end of the synchronization regime for free vibration of a cylinder, with low mass-damping, is generally distinguished by a lower amplitude branch, which has a remarkably constant vibration frequency (f^*_{LOWER}), as typified by Figure 5*b*, and whose frequency level increases as the mass is reduced. Govardhan & Williamson (2000) presented a large data set for the lower branch frequency (f^*_{LOWER}) plotted versus m^*, yielding a good collapse of data onto a single curve fit based on Equation 5:

$$f^*_{LOWER} = \sqrt{\frac{m^* + 1}{m^* - 0.54}}. \tag{12}$$

This expression provides a practical and simple means to calculate the highest frequency attainable by the VIV system in the synchronization regime, if one is provided the mass ratio, m^*. An important consequence of Equation 12 is that the vibration frequency becomes infinitely large as the mass ratio reduces to a limiting value of 0.54. Therefore, Govardhan & Williamson concluded that a critical mass ratio exists

$$\textit{Critical mass ratio}, \quad m^*_{CRIT} = 0.54 \pm 0.02 \tag{13}$$

below which the lower branch of response can never be reached for finite velocities, U^*, and ceases to exist. These conditions are applicable for finite (U^*/f^*), so when the mass of the structure falls below the critical value, one predicts that large-amplitude vibrations will be experienced for velocities U^* extending to infinity:

$$U^*_{end\ of\ synchronization} = 9.25\sqrt{\frac{m + 1}{m - 0.54}}. \tag{14}$$

This expression accurately marks the upper boundary of the shaded synchronization regime in Figure 9*a*. The fact that the critical mass turns out to be 54% is significant because it is in the realm of the "relative densities" of full-scale structures in engineering. We note carefully that this unique value of the critical mass is valid under the conditions of low mass and damping, so long as $(m^* + C_A)\zeta < 0.05$.

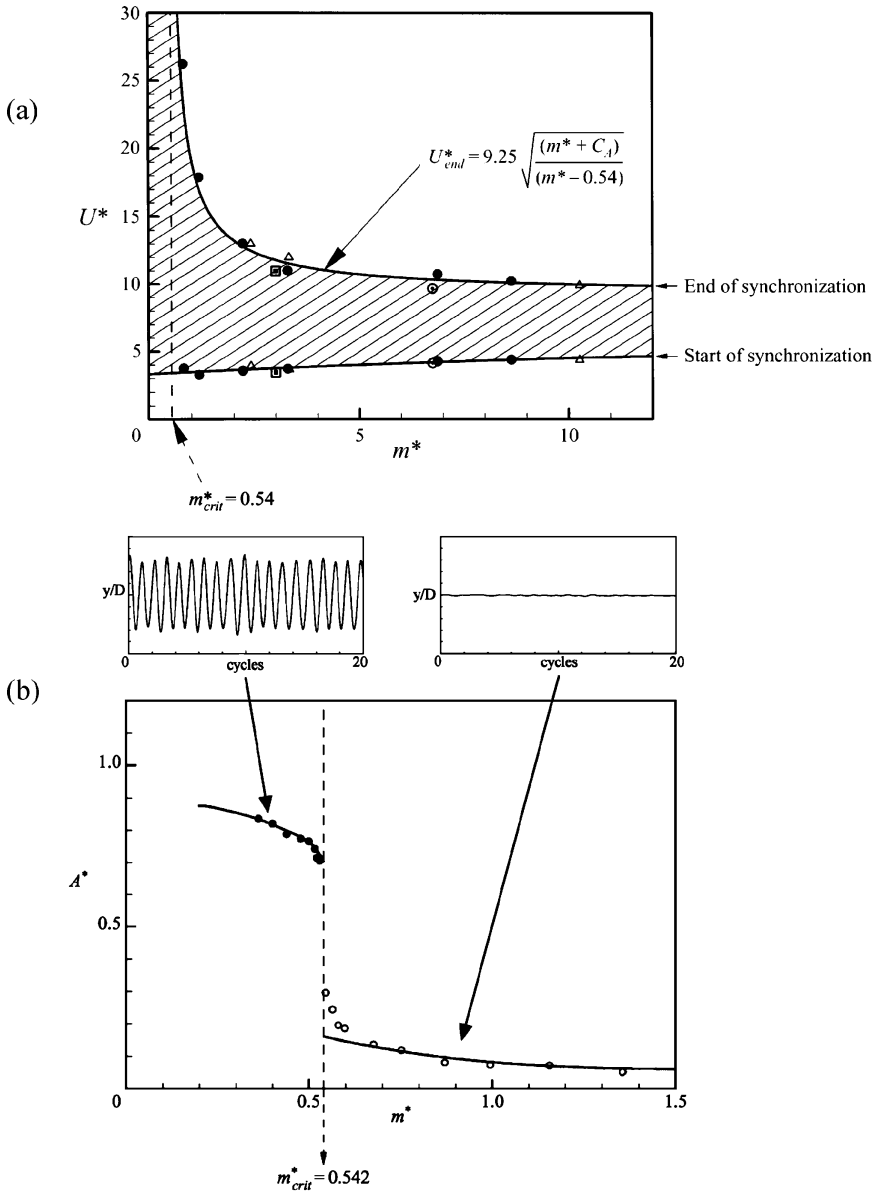

Figure 9 Discovery of a critical mass. The synchronization regime of high-amplitude vibration (*shaded regime*) extends to infinite velocities as m^* approaches the value 0.54, in (*a*) (Govardhan & Williamson 2000). The lower plot in (*b*), from an independent set of experiments at infinite U^*, shows that there is a sudden appearance of large-amplitude response when m^* just falls below 0.54 (Govardhan & Williamson 2002). Symbols in (*a*) are: ●, Govardhan & Williamson (2000); △, Khalak & Williamson (1999); ▣, Hover et al. (1998); ⊙, Anand (1985).

We make the point here that added mass coefficients having a negative value can be observed in data sets collected from forced vibration (see Mercier 1973, Sarpkaya 1978, Gopalkrishnan 1993) and in recent free-vibration data sets (see Vikestad et al. 2000, Willden & Graham 2001). The implications to free-vibration phenomena, such as the possible existence of a "critical mass," were not deduced in these works. However, it has generally been recognized that added mass (or C_{EA}) can predict free-vibration frequencies.

For very small mass ratios, $m^* \sim 1$, as observed by Shiels et al. (2001), Gharib et al. (1997, 1998), Govardhan & Williamson (2000), and Willden & Graham (2001), there is no regime of constant oscillation frequency of the kind observed earlier in Figures 2*b* and 5*b*. The vibration frequency rises almost linearly as U^* increases, which is expected if one considers that the synchronization regime becomes large. There is nothing in principle to suggest that an experiment (consider the $m^* = 0.52$ case in Govardhan & Williamson 2000) cannot reach $U^* \sim 300$, for example, at which point the system will vibrate vigorously at 32 times the natural frequency. This is far from the classical concept of synchronization, where resonant vibration is expected around $U^* \sim 5$–6.

It is possible, even within a laboratory, to take the normalized velocity (U^*) to infinity simply by removing the restraining springs, as done by Govardhan & Williamson (2002). The concept of removing springs is not new; in Shiels et al.'s (2001) numerical simulations they set such structural coefficients (m, c, k) to zero, in their equation of motion. In the experiments, a reduction of mass led to a catastrophic change in response; large-amplitude vigorous vibrations suddenly appear as the mass ratio is reduced to below a critical value, $m^* = 0.542$ (see Figure 9*b*). This accurately proves the prediction of the earlier paper (Govardhan & Williamson 2000); resonant oscillations persist up to infinite (normalized) flow speeds, and in this sense the cylinder resonates forever.

How generic is the phenomenon of critical mass? Govardhan & Williamson (2002) deduced that it will be a universal phenomenon for all systems of VIV whose induced forces and dynamics are reasonably represented by the Equations 1–3. In fact, one finds a critical mass, $m^* \sim 0.30$, for a tethered sphere system (Govardhan & Williamson 2003), a critical mass, $m^* \sim 0.50$, for a pivoted cylinder (Flemming & Williamson 2003), as well as $m^* \sim 0.52$, for an elastically mounted cylinder in two degrees of freedom (Jauvtis & Williamson 2003c). Note that these values are valid for small mass-damping.

4. THE GRIFFIN PLOT

An important question that has been debated for about 25 years is whether a combined mass-damping ($m^*\zeta$) parameter could reasonably collapse peak-amplitude data A^*_{max} in the Griffin plot. The use of a mass-damping parameter stems from several studies. Vickery & Watkins (1964), who considered an equation of motion for flexible cantilevers, plotted their peak amplitudes versus their *Stability parameter* $= K_S = \pi^2 (m^*\zeta)$. Scruton (1965) used a parameter, proportional to K_S,

for his experiments on elastically mounted cylinders that has since been termed the *Scruton number* $= \mathrm{Sc} = \frac{\pi}{2}(\mathrm{m}^*\zeta)$. A slightly different parameter was independently derived from a response analysis involving the van der Pol equation by Skop & Griffin (1973), and they compiled data from several different experiments as a means to usefully predict response amplitudes. The combined response parameter was subsequently termed $\mathrm{S_G}$ in Skop (1974), and is defined here as

$$\textit{Skop-Griffin parameter} = \mathrm{S_G} = 2\pi^3\mathrm{S}^2(\mathrm{m}^*\zeta). \tag{15}$$

As a side note, the late Dick Skop (private communication) wrote to us stating that the well-known $\mathrm{S_G}$ initials actually represented the researchers Skop and Griffin, a fact that is not generally known. Griffin et al. (1975) made the first extensive compilations of many different investigations, using $\mathrm{S_G}$, and subsequently the classical log-log form of the plot (Griffin 1980), as shown in Figure 3*c*, has become the widely used presentation of peak response data. Despite the extensive use of the log-log Griffin plot by practicing engineers, it is not known precisely under what conditions the assumptions regarding $(\mathrm{U}^*/\mathrm{f}^*)$ and f^* would hold, that would lead to a unique curve of $\mathrm{A}^*_{\mathrm{max}}$ versus $\mathrm{S_G}$, as discussed in Section 1.

Perceived problems regarding the validity of this widely used plot were pointed out clearly in a number of papers by Sarpkaya (1978, 1979, 1993, 1995). He stated that simple observation of his equation of motion (equivalent to Equation 1) showed that "one must conclude that the dynamic response is governed, among other parameters, by m^* and ζ independently, not just by $(\mathrm{m}^*\zeta)$." On the basis of the analysis of three data points, Sarpkaya (1978) suggested that one should use the combined parameter $\mathrm{S_G}$ only if $\mathrm{S_G} > 1.0$, which rules out most of the plot, as one can see in Figure 3*c*.

On the other hand, Griffin & Ramberg (1982) performed two sets of experiments, each for the same value of $\mathrm{S_G} = 0.5$–0.6, but with dissimilar mass ratios, $\mathrm{m}^* = 4.8$ and 43. These data demonstrate two points. First, the lower mass ratio leads to a wider synchronization regime, extending over a larger range of normalized velocity U^*. Second, at the same $\mathrm{S_G}$, the peak amplitude is roughly unchanged at $A^*_{\mathrm{max}} = 0.5$, despite the fact that $\mathrm{S_G} < 1.0$.

If we plot an extension of the Griffin plot for a variety of experiments compiled by Skop & Balasubramanian (1997) but in this case using a linear Y-axis in Figure 10*a*, we see significant scatter, otherwise masked by the classical log-log format. An update of Table 1 from Khalak & Williamson (1999) indicates that the maximum attainable amplitude lies anywhere in the range $\mathrm{A}^* = 0.8$–1.6. Given this scatter, it does not appear reasonable to collapse data for such different VIV systems (free cylinder, cantilever, pivoted cylinders, etc.) in the same plot.

In Figure 10*b* we present only those data corresponding to elastically mounted cylinders. Following Khalak & Williamson (1999), we introduce two distinct curves into the Griffin plot representing the peak amplitudes for both the upper and the lower branches. The resulting data from these diverse experimental arrangements appear to give an approximate functional relationship between $\mathrm{A}^*_{\mathrm{max}}$ and $(m^* + C_A)\varsigma$ over a wide range of parameters; applicable for the regime

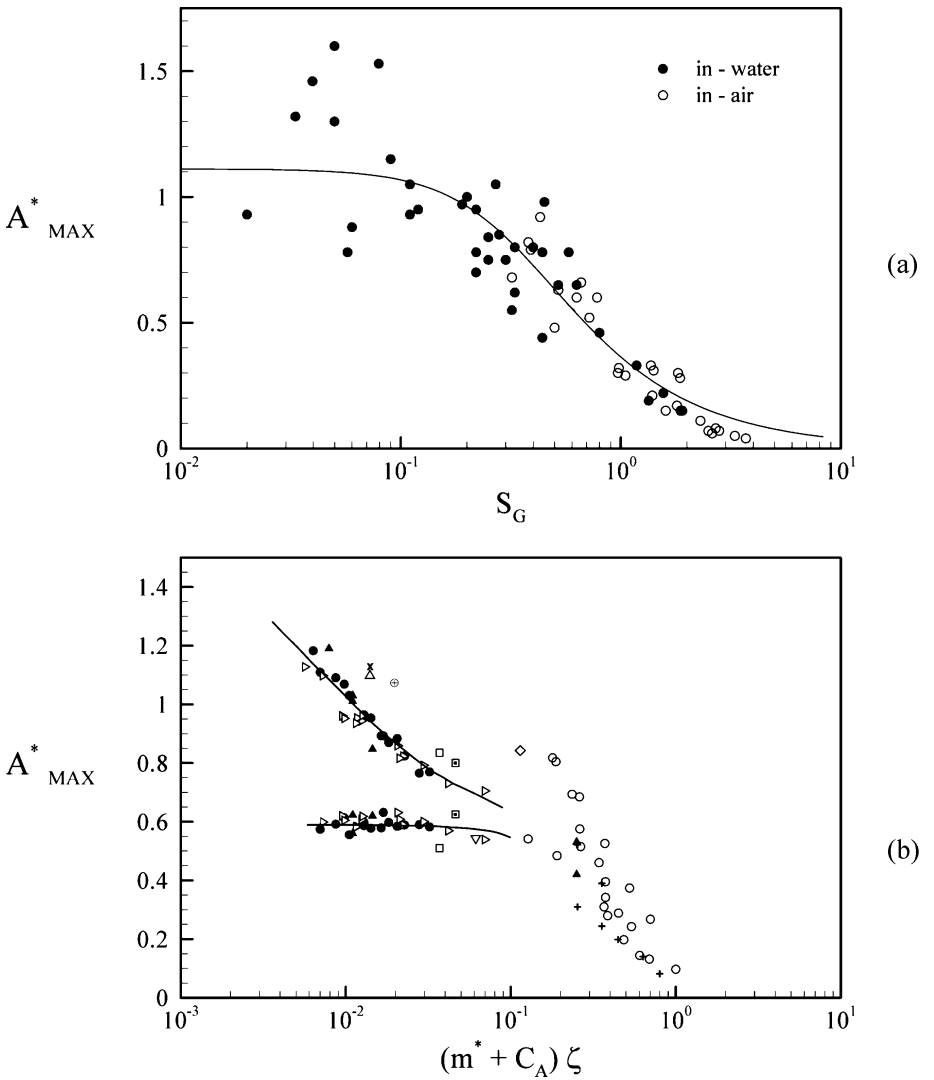

Figure 10 The Griffin plot. (*a*) presents peak-amplitude data versus Skop-Griffin parameter (S_G) collected by Skop & Balasubramanian (1997), with more recent data (see Table 1), along with curve fits through the data. This indicates a large scatter. By removing those data for different vortex-induced vibration systems, in (*b*), one can demonstrate the reasonable collapse of data for elastically mounted cylinders (only). In (a), — is Equation 16 with best-fit $B = 0.385$; $C = 0.120$. Symbols in (b) are: ●, Khalak & Williamson (1999); ▲, Govardhan & Williamson (2000); ◘, Hover et al. (1998); ○, Griffin (1980); ▷, Jauvtis & Williamson (2003); △, Moe & Overvik (1982); ▽, Angrilli et al. (1972); □, Owen (2001); ◇, Gharib et al. (1998); +, Feng (1968); ×, Vikestad (1998); ⊕, Anand & Torum (1985).

TABLE 1 Peak-amplitude data

Investigators	Year	Medium	Re	$m^*\zeta$	A^* (peak)
(A) Elastically-mounted rigid cylinders (Y-only)					
Angrilli et al.	1974	Water	2,500–7,000	0.049	0.54
Dean et al. (1)	1977	Water	2,800–10,200	0.0055	0.94
Moe & Overvik	1982	Water	6,000–30,000	0.013	1.09
Anand & Torum	1985	Water	6,500–35,000	0.013	1.07
Sarpkaya	1995	Water	6,000–35,000	0.052	0.95
Gharib et al.	1998	Water	11,000–40,000	0.094	0.84
Hover et al. (2)	1998	Water	3,800	0.040	0.80
Khalak & Williamson	1999	Water	5,000–16,000	0.0047	1.18
Govardhan & Williamson	2000	Water	2,900–19,000	0.0027	1.19
Vikestad et al.	2000	Water	14,000–65,000	0.012	1.13
Owen et al.	2001	Water	1,650–7,500	0.036	0.84
Jauvtis & Williamson	2003a	Water	5,000–13,000	0.0048	1.13
(B) Elastically mounted rigid cylinders (XY-motion) (3)					
Jauvtis & Williamson	2003c	Water	7,200–15,400	0.0064	1.50
(C) Cantilevers and Pivoted Cylinders					
Vickery & Watkins (4)(5)	1964	Water	7,000	0.016	1.46
King (5)	1974	Water	6,000–22,500	0.020	1.60
Pesce & Fujarra (5)	2000	Water	6,000–40,000	0.013	1.32
Fujarra et al. (5)(6)	2001	Water	1,000–2,500	0.023	0.78
Flemming & Williamson (7)	2003	Water	500–2,000	0.032	1.53
(D) Forced oscillations of cylinders (Amplitude limit of positive excitation)					
Mercier	1973	Water	2,000–33,000		1.10
Sarpkaya	1978	Water	5,000–25,000		0.90
Hover et al.	1998	Water	3,800		0.82
(E) Low-Re experiments					
Anagnostopoulos & Bearman	1992	Water	90–150	0.179	0.55
(F) Direct Numerical Simulation (DNS)					
Blackburn & Karniadakis (8)	1993	2-D Code	200	0.012	0.64
Newman & Karniadakis (8)	1995	2-D Code	200	0.00	0.65
Shiels et al.	2001	2-D Code	100	0.00	0.59
Fujarra et al.	1998	2-D Code	200	0.015	0.61
Guilmineau & Queutey	2000	2-D Code	100	0.179	0.54
Blackburn et al.	2001	2-D Code	430–560	0.122	0.47
Evangelinos & Karniadakis	1999	3-D Code	1,000	0.00	0.74
(G) Turbulence Models (LES and RANS)					
Saltara et al. (LES)	1998	2-D Code	1,000	0.013	0.67
Guilmineau & Queutey (RANS)	2002	2-D Code	3,800	0.013	0.98

Notes regarding these collected data.

(1) Amplitude response plots show multiple peaks and large scatter.

(2) Virtual free-vibration experiments using real-time force-feedback control system.

(3) Cases where oscillating mass and natural frequency in both directions are identical.

(4) Vickery & Watkins performed experiments with an adjustable cantilever/pivoted cylinder, and not simply a pivoted cylinder (as usually quoted).

(5) The peak A/D here is less than the tip amplitude, and uses a modal parameter as defined in Griffin, Skop & Ramberg (1975).

(6) Restricted to transverse Y-motion only.

(7) Pivoted cylinder with two degrees of freedom.

(8) X-Y motions were simulated (two degrees of freedom).

$m^* > 2$, and for $(m^* + C_A)\zeta > 0.006$. There seems to be a regime of validity for the Griffin plot that extends to two orders of magnitude lower mass-damping (down to $S_G \sim 0.01$) than the limits ($S_G > 1$) suggested by Sarpkaya, and often quoted in the literature.

Equations to fit the compiled data in the Griffin plot have been put forward by several investigators whose complicated empirical functions are listed in Blevins (1990; see Table 3-2 therein). Sarpkaya (1978) used an equation of motion for the vibrating structure to formulate a more simple and useful empirical equation relating A^*_{MAX} to S_G, as follows

$$A^*_{MAX} = \frac{B}{\sqrt{C + S_G^2}}. \tag{16}$$

Note that B and C are not strictly constants. (The value of B is proportional to force coefficient C_Y, and Sarpkaya noted that C_Y depends on A^*.) The resulting best-fit curve (with $B = 0.385$ and $C = 0.120$) is plotted in Figure 10*a*, and serves reasonably well to represent the data, although it is difficult to validate in the presence of such large scatter of the data. However, we show in Section 6 that Sarpkaya's formula fits very well the data for low Reynolds numbers, in the laminar vortex formation regime.

Finally one might observe in Figure 10*b* that, even for the smallest mass-damping, the peak amplitudes are not yet close to saturating at a specific value. One might ask: What is the maximum attainable amplitude that can be reached as $(m^* + C_A)\zeta$ gets ever smaller? The largest peak amplitude achieved so far in the Griffin plot is $A^* = 1.19$, but the trend of the data suggests this is not the limit. One can conclude that, despite the enormous effort over the last 25 years to critique and define accurately this useful plot, it is not yet fully defined.

5. FORCED VIBRATION OF A CYLINDER

One approach to predicting VIV has been to generate an experimental force data base by testing cylinders undergoing forced or controlled sinusoidal oscillations in a free stream. Several investigators, including Bishop & Hassan (1964), Mercier (1973), Sarpkaya (1977, 1978), Staubli (1983), Gopalkrishnan (1993), and more recently Hover et al. (1997, 1998), Sheridan et al. (1998), and Carberry et al. (2001, 2003a,b,c), have measured the forces on bodies in harmonic, as well as multifrequency motion. As mentioned in Section 1 in conjunction with Sarpkaya's well-known data set, in these experiments the transverse force is generally decomposed into two components, one in phase with the velocity ($C_Y \sin\phi$, which predicts when free vibration should occur) and one in phase with the acceleration ($C_Y \cos\phi$, which yields the effective added mass).

Predictions using controlled vibration data with an assumed equation of motion have been compared with free-vibration tests (Parkinson 1974, Sarpkaya 1978, Staubli 1983). Staubli built up a complete response plot to match Feng's (1968)

free-vibration experiments. There are parametric regions where such comparison is successful, and other regions where the comparison is not close. For example, Carberry et al. (2003a,b) found that cases where free vibration shows the excitation is obviously positive might be contrasted with equivalent cases in the forced vibrations (with strictly sinusoidal motion), where energy transfer is negative.

Hover et al. (1997, 1998), in conjunction with Michael Triantafyllou's research group at MIT, developed an ingenious and extremely versatile experiment, namely a novel force-feedback Virtual Cable Testing Apparatus (VCTA). The system, mounted on a carriage over the MIT Towing Tank, comprises (*a*) a computer using a measured force signal from the test cylinder to drive in real time a numerical simulation of an equivalent mass-dashpot-spring system, and (*b*) a servomotor that imposes the computed motion to the submerged cylinder. Figure 11*a*, from Hover et al. (1998), shows contours of excitation ($C_Y \sin\phi$), and there is a remarkable agreement between the superposed free-vibration response plot (symbols) for almost zero damping, and the contour of zero excitation ($C_Y \sin\phi = 0$). These results have all been superposed on the Williamson & Roshko map of vortex mode regimes.

One of the many interesting results from this novel apparatus is that the correlation between force transducers at each end of the cylinder is high in general, with the exception of the region of maximum amplitude, suggesting a 3D vortex formation process for the upper-lower branch transition (Hover et al. 2003). Correlation is clearly important when predicting VIV. The versatile force-feedback system is also used to look at multimode motions, traveling waves, and structural nonlinearities; parameters need only be changed in software!

The combined groups of Don Rockwell at Lehigh University and John Sheridan of Monash University recently made extensive measurements of force from controlled vibrations of cylinders, resulting in a number of papers (Sheridan et al. 1998 and Carberry et al. 2001, 2003a,b,c). Carberry et al. (2001) showed conclusive evidence that the force phase shift (jump in ϕ) is associated with the change in vortex pattern from a low-frequency (low-f) mode to a high-frequency (high-f) mode of vortex formation. This is in direct agreement with the conclusions from free vibration in Govardhan & Williamson (2000). Thus, Carberry et al.'s (2003b) paper compares directly the controlled vortex modes (see Figure 11*b*) with these free-vibration modes. The low-f mode is a 2P mode, while the high-f mode is the 2S vortex wake mode. Carberry et al. (2003a,b,c) also discovered an intermediate mode, which is the equivalent of the upper branch 2P mode in free vibration. Govardhan & Williamson (2001) studied the mean velocity and mean vorticity for the various modes, noting the clear departure from the classical near wake recirculation regime for the 2S mode type of wake, and the appearance of a downstream jet-like near wake structure (for the 2P mode). Carberry et al. (2003b,c) found mean vorticity plots from corresponding forced vibration studies (included in Figure 11*c)*, indicating such a jet flow. In summary, despite the extensive work on controlled vibrations, it is still an open question whether (strictly sinusoidal motion) controlled experiments can be used to predict free vibration accurately.

6. LAMINAR VORTEX-INDUCED VIBRATION

There is only one free-vibration experiment, to our knowledge, that has been conducted within the laminar vortex shedding regime, and it is described in the paper by Anagnostopoulos & Bearman (1992), over a range, Re = 90–150. Their response amplitude plot corresponds very well with the results from a much larger number of two-dimensional numerical simulations at Re = 100–200 (for example, Blackburn & Karniadakis 1993; Anagnostopoulos 1994; Newman & Karniadakis 1995, 1996; Saltara et al. 1998; Evangelinos & Karniadakis 1999; Shiels et al. 2001; Zhou et al. 1999; and others; see Table 1*F*).We directly compare selected response plots, for the first time, in Figure 12*a*. Not only is the comparison remarkably good between experiment and computation, but we demonstrate the existence of a possible hysteresis at the low-velocity end of the synchronization regime, which apparently has not been discussed previously. These data correlate well with the map of regimes for low Reynolds numbers, shown in Figure 12*b*, adapted from Meneghini & Bearman (1993). These authors also demonstrated that the 2S mode persists up to a level of $A^* = 0.6$, beyond which they found the P+S mode, in agreement with Griffin & Ramberg's (1974) classical smoke visualizations. There is a striking agreement in Figure 13 between simulations and experiment for the P + S mode, as distinct from the 2S mode. (Please see Note Added In Proof for recent findings regarding the laminar map of regimes.)

We conclude that there is a clear correspondence between the nonexistence of any free-vibration amplitude A^* in excess of 0.6, even in the case of the simulations where damping can be set to zero, with the fact that the vortex wake mode changes over to the P + S mode. Unlike the 2P mode, which only appears when the shedding becomes turbulent for Re > 200 (Williamson & Roshko 1988), the P + S mode apparently does not deliver a net positive energy of excitation enabling free vibration.

Finally, in Figure 12*c*, we present a Griffin plot, dedicated to the laminar regime, where typically Re < 200 (see Table 1*E*,*F*). It is immediately apparent that the maximum amplitudes saturate at $A^* \sim 0.6$. Given the excellent definition of this data, we represent it by the curve fit of Sarpkaya (Equation 16, with B = 0.1470,

Figure 12 Laminar vortex-induced vibration response (Re < 200). In (*a*), we compile sets of response amplitude data from different investigators into one plot, indicating good agreement, and also a possible hysteresis. There is a good correspondence with the map of modes, adapted from Meneghini & Bearman (1993), in (*b*). The Griffin plot can now be accurately defined in (*c*), yielding a saturation amplitude of $A^* \sim 0.6$. Symbols in (*a*) and (*c*) are: ●, Anagnostopolous & Bearman (1992); ○, Anagnostopolous (1994); □, Newman & Karniadakis (1997); △, Shiels, Leonard & Roshko (2001); ▷, Willden & Graham (2000); ▽, Guilmineau & Queutey (2000); ◁, Fujarra et al. (1998); ◇, Blackburn & Karniadakis (1993); +, Blackburn et al. (2001).

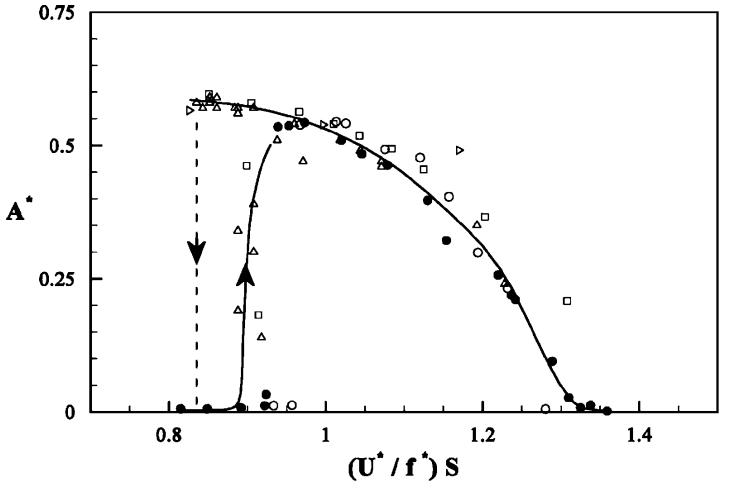

(a)

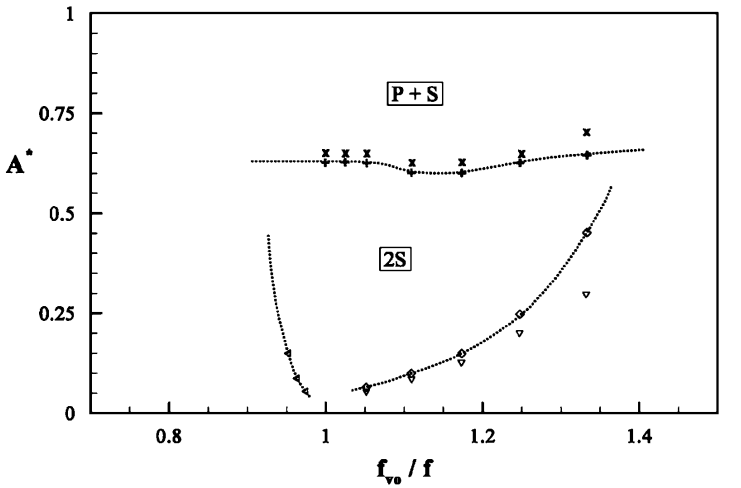

(b)

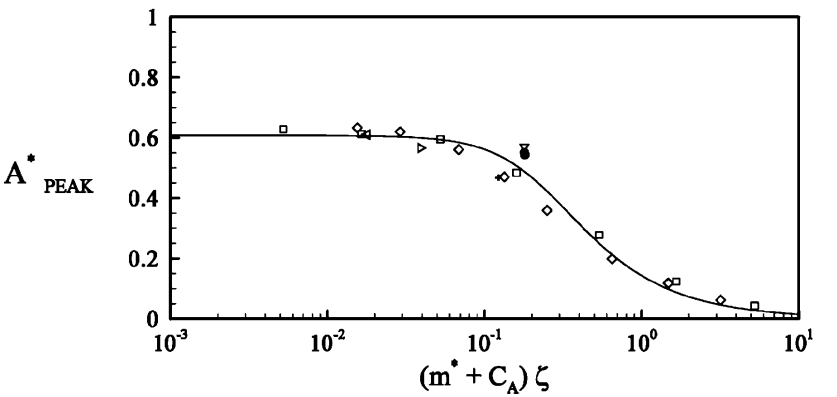

(c)

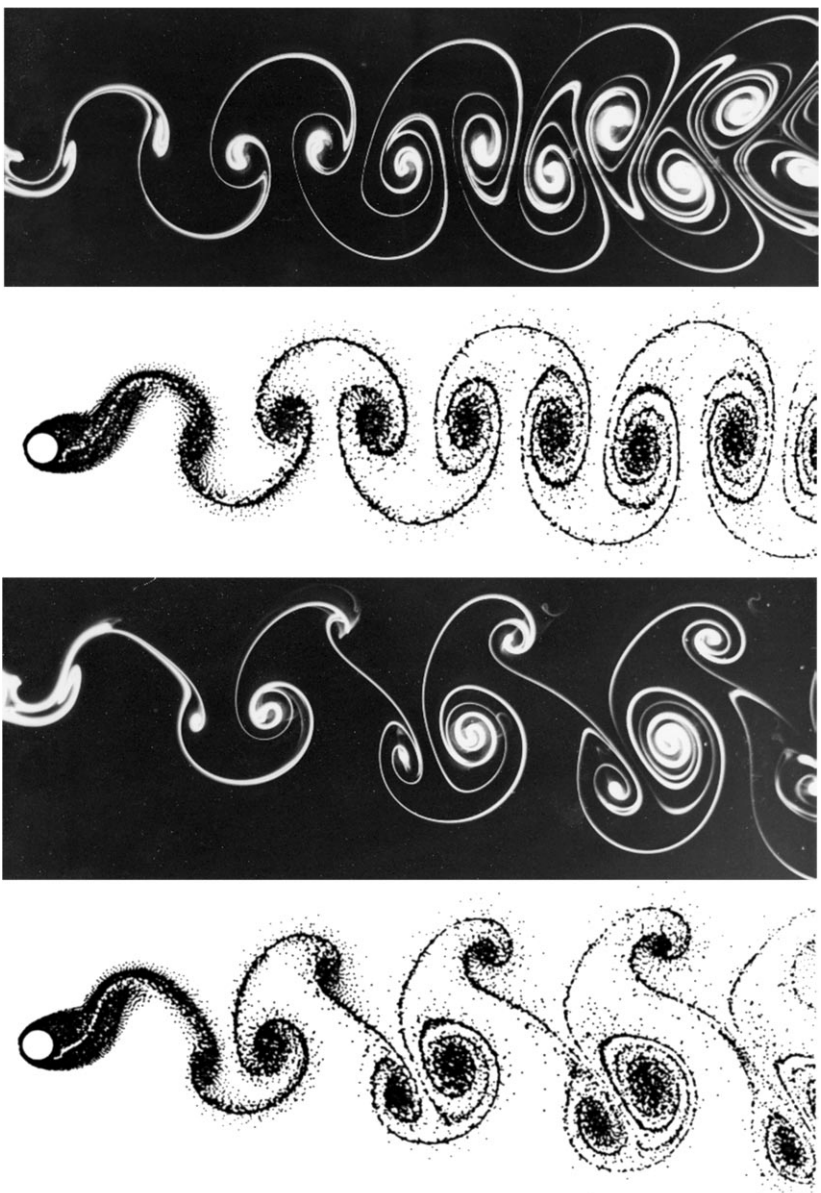

Figure 13 Direct comparison between the 2S and P + S vortex modes between experimental dye visualizations (Williamson 1987, unpublished) and numerical simulations (Meneghini & Bearman 1995), illustrating a remarkable agreement. Such visualizations can only be seen clearly in the laminar regime (Re < 200).

C = 0.0585), yielding a good fit and thus demonstrating the usefulness of this empirical function to represent peak-amplitude data in the Griffin plot.

7. THE LEONARD-ROSHKO-SHIELS "EFFECTIVE ELASTICITY"

Illuminating ideas have come from the computational approach of Tony Leonard and Anatol Roshko's group at Caltech, triggered by the unique possibility in simulations to set mass, damping, and stiffness (or any combination of these) to precisely zero, in the equation of motion of an elastically mounted cylinder, at Re = 100. This has led directly to a new single-parameter formulation for the response, involving a quantity they have defined as the "effective elasticity." These researchers (Roshko et al. 2000, Shiels et al. 2001, Leonard & Roshko 2001) adopted a different scaling for the equation of motion than conventionally employed; rather than the mechanical quantities {m, c, k}, they used the flow quantities {U, ρ, μ} to normalize their equation:

$$m^*y^* + b^*y^* + k^*y^* = C_Y(t^*), \tag{17}$$

where the terms are laid out clearly in Shiels et al. (2001). (Note that m^* and f^* are defined differently here.) If one sets all the mechanical coefficients to zero: $m^* = b^* = k^* = 0$, then the resultant transverse force is zero: $C_Y(t^*) = C_{YA}(t^*) + C_{YW}(t^*) = 0$, so if the body moves, it will have to satisfy a balance between the added mass force $C_{YA}(t^*)$ and the vortex wake force $C_{YW}(t^*)$ at all times. Despite the fact that the body is completely disconnected with the mechanical system (although restrained streamwise), it vibrates at a significant amplitude ($A^* = 0.47$), with a frequency of vibration given by (fD/U) = 0.156, close to the fixed-body result. This is a remarkable result! The vorticity dynamics are illustrated beautifully by the image in Figure 1*b*.

If one continues to assume that the damping is zero, $b^* = 0$, one can write the equation of motion, with the assumption of sinusoidal force ($C_Y = C_L \sin \omega^* t^*$) and response ($y^* = A^* \sin \omega^* t^*$), as follows:

$$[-\omega^{*2}m^* + k^*]A^* = k_E^* A^* = C_L. \tag{18}$$

The inertial and spring terms in the equation (which are precisely out-of-phase) are combined into an "effective elasticity" = k_E^*, and thus the amplitude and frequency $\{A^*, f^*\}$ are dependent on this parameter, as Figure 14 shows (Leonard & Roshko 2001). The same response plot is also applicable for any value of the mass, m^*. Given the assumption of zero damping, one has a useful reduction of variables in the problem, from three variables: $A^* = f\{m^*, b^*, k^*\}$, to one variable: $A^* = g\{k_E^*\}$.

As Leonard & Roshko (2001) stated, the mechanical parameters are "hidden" in the solutions. In fact, one can generate a set of "mapped" response plots, using

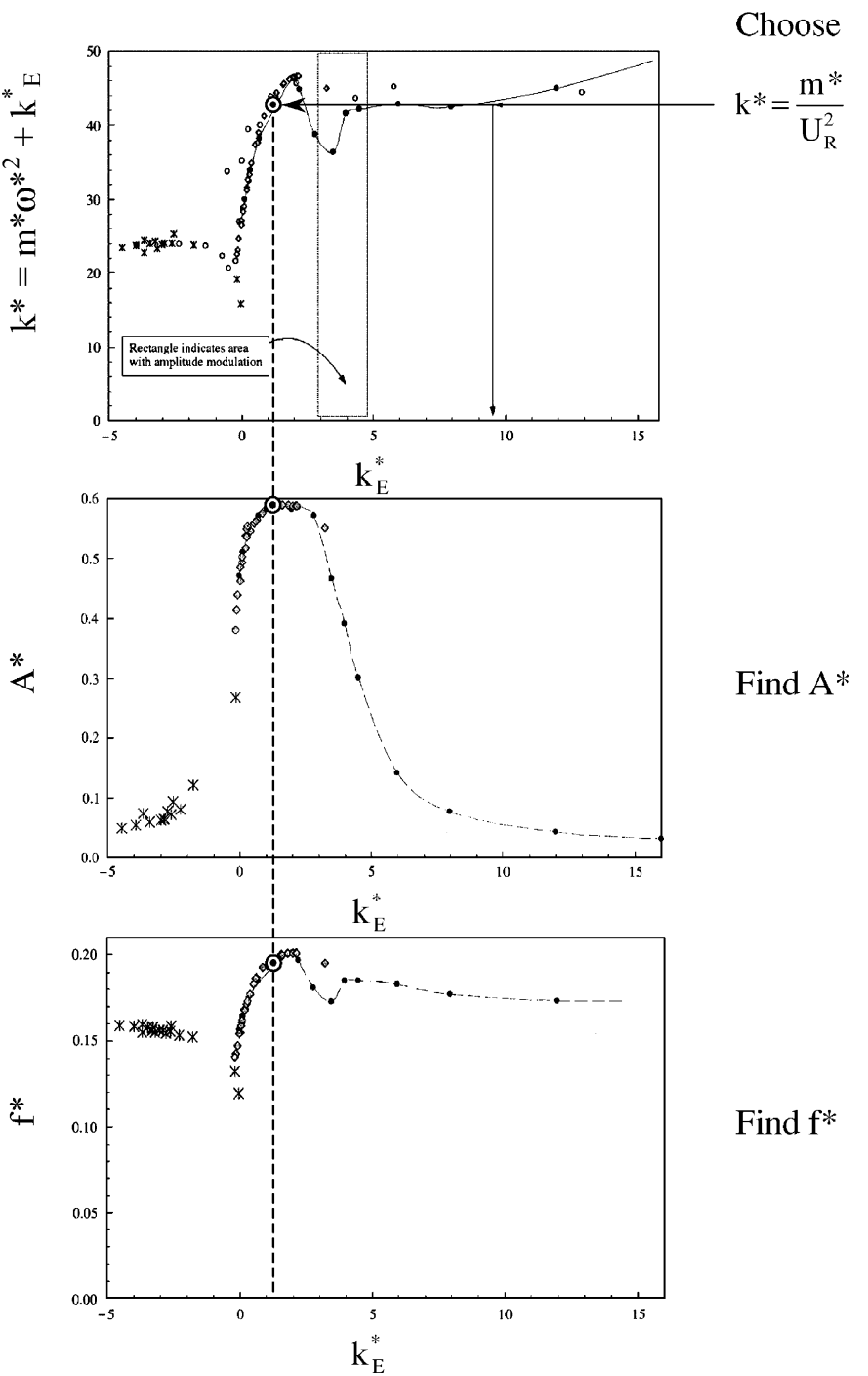

the data in Figure 14. If one chooses a particular mass ratio (m^*), then one can deduce the amplitude (A^*) and frequency (f^*) as a function of U^* (the traditionally used velocity), and build up a complete response plot for the chosen m^*.

8. XY MOTION OF BODIES

Despite the large number of papers dedicated to the problem of a cylinder vibrating transverse to a fluid flow (Y motion), there are very few papers that also allow the body to vibrate in-line with the flow. One principal question that may be posed is: How does the freedom to vibrate in-line with the flow influence the dynamics of the fluid and the structure?

In most past experimental work with XY vibrations (Moe & Wu 1990, Sarpkaya 1995), the mass ratios and natural frequencies were chosen to have different values, except for one data set for the same frequency in Sarpkaya. Under their chosen special conditions, these studies demonstrated a broad regime of synchronization, similar to Y-only studies, but with no evidence of the different response branches. Sarpkaya concluded from his work that bodies in XY motion do not lead to surprising changes in the expected maximum resonant amplitudes as compared to bodies in Y motion. Jeon & Gharib (2001) recently adopted a different approach, forcing a cylinder to move in the X and Y directions, in a fluid flow, under the prescribed motions given by $x(t) = A_X \sin(2\omega t + \theta)$; $y(t) = A_Y \sin(\omega t)$. Specific phase angles $\theta = 0^\circ$ and -45° were chosen because they stated that "nature prefers a figure-eight type motion." One of the most interesting results from Jeon & Gharib's study is that even small amounts of streamwise motion ($A_X/A_Y = 20\%$) can inhibit the formation of the 2P mode of vortex formation. Note that in Jauvtis & Williamson's (2003c) free-vibration study, body motions exist that can be different from a figure-eight motion. Clearly, the selection of amplitudes and phases will influence the resulting conclusions.

Full-scale piles in an ocean current (Wooton et al. 1972), and similar cantilever models in the laboratory (King 1974), vibrate in-line with the flow with peak amplitudes of the cantilever tip ($A^*_X \sim 0.15$). As Bearman (1984) and Naudascher (1987) noted, oscillations ensue if the velocity is close to $U^* \sim 1/2S$. King (1974) showed a classical vortex street (antisymmetric) pattern, although these investigators also discovered a second mode where the wake formed symmetric vortex pairs close to the body. One subsequent approach, where these two modes have been observed, is to vibrate bodies in-line with the flow (Griffin and Ramberg 1976, Ongoren & Rockwell 1988b). Ongoren & Rockwell also demonstrated a

Figure 14 The Leonard-Roshko-Shiels "effective elasticity," k^*_E, which permits a collapse of data for very "light" damping ($b^* \sim 0$), and allows the definition of mapped response plots {A^* or f^*} versus U^*, for any chosen mass ratio, m^*. From Leonard & Roshko (2001).

P + S type of mode, although this was not seen in streamwise free-vibration studies. Numerical investigations at low Reynolds numbers (for example, Blackburn & Karniadakis 1993, Newman & Karniadakis 1995, Zhou et al. 1999), which generally observe figure-eight trajectories, demonstrate that there does not appear to be much influence on the forces if one also allows streamwise body motion.

In most practical cases, cylindrical structures (such as riser tubes or heat exchangers) have the same mass ratio and the same natural frequency in both the streamwise (X) and transverse (Y) directions. Two recent arrangements that ensure such conditions are the air bearing platform of Don Rockwell's group at Lehigh University (Leyva et al. 2003), and a pendulum setup at Cornell (Jauvtis & Williamson 2003a,b,c). Both studies demonstrate a set of response branches, in contrast to previous XY experiments. Even down to the low mass ratios, where $m^* = 6$, it is remarkable that the freedom to oscillate in-line with the flow hardly affects the response branches, the forces, and the vortex wake modes. These results are significant because they indicate that the extensive understanding of VIV for Y-only body motions, built up over the last 35 years, remain strongly relevant to the case of two degrees of freedom.

However, there is a dramatic change in the fluid-structure interactions when mass ratios are reduced below $m^* = 6$. A new response branch with significant streamwise motion appears in what Jauvtis & Williamson (2003b,c) defined as the "super-upper" branch, which yields massive amplitudes of three diameters peak-to-peak ($A^*_Y \sim 1.5$), as seen in Figure 15. This response corresponds with a new periodic vortex wake mode, which comprises a triplet of vortices being formed in each half cycle, defined as a "2T" mode following the terminology that Williamson & Roshko (1988) introduced.

9. "COMPLEX FLOWS": FLEXIBLE, TAPERED, PIVOTED, AND TETHERED BODIES

As bodies become more directly practical, they generally become more complex, although many of the phenomena discovered for the simpler paradigm of the elastically mounted cylinder carry across to more involved structures, including those whose vibration amplitude varies along the span. For example, in the case of flexible cantilevers, the recent work of Pesce & Fujarra (2000) and Fujarra et al. (2001) indicates that there is an initial branch of (tip) amplitude response, which has a hysteretic transition to a lower branch, similar to the elastically mounted or free cylinder. Techet et al. (1998) discovered a 2S-2P Hybrid mode (shown in Figure 16*a*), comprising the 2S and 2P modes occurring along different spanwise lengths of their tapered cylinder, with vortex dislocations between the spanwise cells. They showed an excellent correlation and prediction of these modes in the framework of the Williamson & Roshko (1988) map of modes.

Vortex-induced vibrations of pivoted cylinders also exhibit similar branches of response to the cantilever and free cylinder, as seen from Balasubramanian et al.

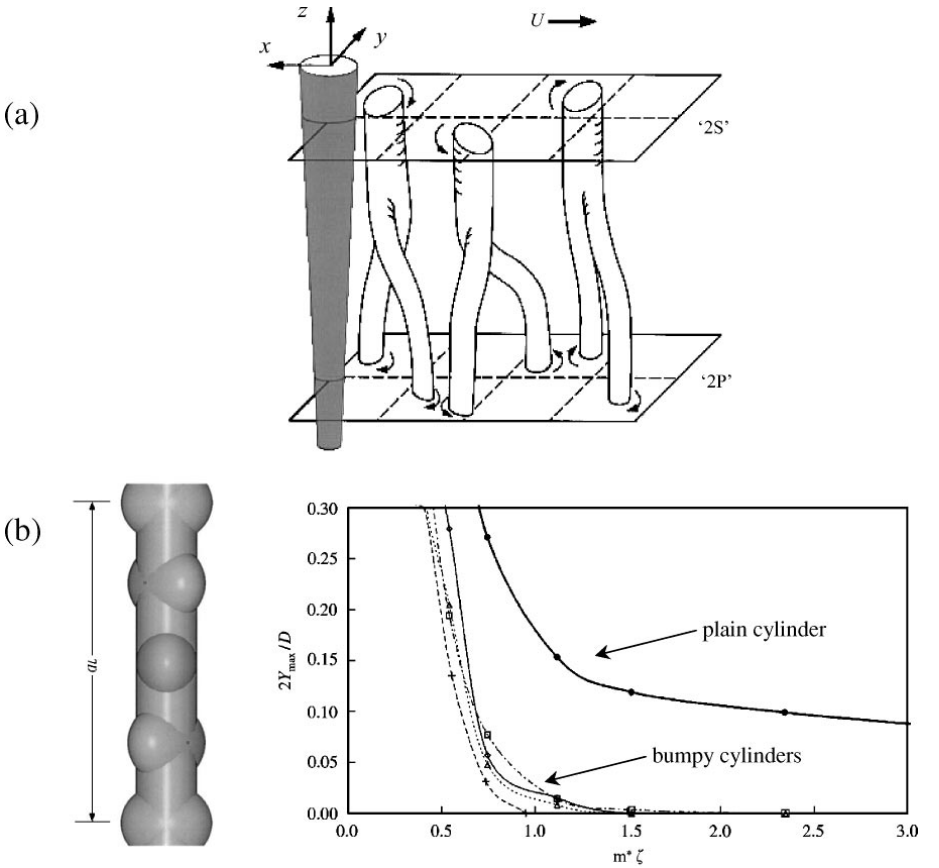

Figure 16 (*a*) shows the Techet et al. (1998) "2S-2P Hybrid" mode, comprising spanwise regimes of 2S and 2P modes, separated by periodic vortex dislocations, for a controlled transverse vibration of a tapered cylinder. In (*b*), the "bumpy" cylinder of Owen et al. (2001) provides vortex-induced vibration (VIV) suppression until a sufficiently low mass-damping ($m^*\zeta$) is reached when VIV resumes.

(2000) and Weiss & Szewczyk (2000), who studied many scenarios, comprising uniform and nonuniform cylinders in uniform or sheared flows. They indicate the broadening of the response regime and reduction in tip amplitude ($A^* \sim 0.3$) for sheared flows, and an interesting case where the taper and shear effects cancel each other to yield the most uniform vortex shedding along the span, and hence an increased response. Voorhees & Wei (2002) observed some similar modes to those of the "free" cylinder (see also Dong et al. 2003), for their pivoted cylinder, and investigated the effects of spanwise flows. These studies confine vibrations to transverse motion, but Flemming & Williamson (2003) recently studied the case of a pivoted cylinder free to move streamwise as well as transverse to the flow.

Over a range of body inertias I^* (equivalent to m^*), a number of different spanwise modes were discovered. For cases with high I^*, and negligible streamwise motion, either the 2S or 2P modes were observed along the span, but for lighter structures, the Techet et al. 2S-2P Hybrid mode was found. Finally, Flemming & Williamson discovered a distinct new mode along the span, comprising two corotating vortices formed each half cycle, namely the "2C" mode in Figure 17*b*, for the lightest of their structures. For this case, they also found three response amplitude branches, which need to be plotted in a 3D version of the Williamson & Roshko map (in Figure 17*a*) to indicate that the crossover of branches (upper and lower) actually occur at different heights (different A_X^*). The higher branch corresponds with the "2C" mode.

Kim Vandiver at MIT has undertaken extensive field and laboratory experimental studies concerning cable dynamics (see for example, Vandiver 1993, Vandiver & Jong 1987), and he has developed a well-known cable VIV prediction program "SHEAR 7" (Vandiver 2003) that is currently based on data for short laboratory cylinders. There are several ongoing validation studies, which consider multimode response, as described by Vandiver & Marcollo (2003), including some upcoming large-scale towed cable experiments to be conducted in Seneca Lake, NY ("Deepstar" joint industry program). Marcollo & Hinwood (2002) have just completed related experiments involving a cable in uniform flow, where they find evidence for similar added mass values and response branches as those found for short cylinders.

The group of George Karniadakis at Brown University have performed extensive computational studies, beginning with their studies to investigate laminar flow past a freely vibrating cable (Blackburn & Karniadakis 1993; Newman & Karniadakis 1995, 1996, 1997). In these cases, they employed a simple wave equation to model the structure and found two possible wake states: one for a traveling wave (oblique vortices), and one for a standing wave response (Lambda-shaped vortices). The potential of 3D computational studies is perhaps illustrated by the simulation in Figure 18*a* showing the different types of vortex formation discovered at the nodes and antinodes of the cable undergoing standing wave vibration. Subsequent works (for example, Evangelinos & Karniadakis 1999) developed a new class of spectral methods suitable for unstructured and hybrid grids. They computed a mixed response mode, comprising oblique and parallel shedding, caused by modulated traveling wave motion, whose effect on the lift force distribution has been studied. Lucor et al. (2001) investigated very long bodies (aspect ratio >500) in uniform and sheared flows to observe vortex dislocations of the kind found for fixed-body flows (Williamson 1992), which cause substantial modulation of lift forces. Figure 18*b* illustrates the intricate type of cable response, where the time history of the distribution of transverse displacement is exhibited, for a standing wave pattern in an exponential shear distribution.

Modeling the flow and vibrations of cables recently received a renewed interest. Triantafyllou & Grosenbaugh (1995) were able to usefully compute cable dynamics with an empirical model of the lift force excitation as a linear function of the

amplitude. This group also has been exploiting the unique Virtual Cable Testing Apparatus (Section 5) to study dynamic response for multimode models, arising from inclined cable dynamics (Hover et al. 1997). Skop & Balasubramanian (1997) and Skop & Luo (2001) undertook extensive modeling of spanwise vortex shedding and structure dynamics of cylinders in uniform and sheared flows using van der Pol type oscillators, with a coupling term proportional to body velocity.

In a systematic paper, Facchinetti et al. (2003) studied the effect of a coupling term between the equation for near wake dynamics (van der Pol), and the one degree-of-freedom structure oscillator. They found good comparison between their model and the recent results of Govardhan & Williamson (2000) and Vikestad et al. (2000), but perhaps the principal conclusion is that the optimal coupling term involves the body acceleration, rather than the displacement or velocity. This is a useful result for future modeling developments. Facchinetti et al. (2002) also observed cellular shedding (of the kind found experimentally in Stansby 1976), and they were able to suppress VIV with their model. Facchinetti et al. (2003) also looked into the problem of vortex-induced waves (VIW), using both their modeling approach and also experiment. Kim & Perkins (2002) studied other cable models, showing the essential character of experimental VIV response, including hysteresis. Finally, Willden & Graham's (2001) approach is unique in that they developed an efficient "quasi-3D" simulation, where the two-dimensional flow is computed at various spanwise locations, and these are linked by a three-dimensional large-scale vortex lattice representation. In the case of sheared flows, their method yields cellular shedding, in agreement with other modeling results, and with the experimental work of Stansby (1976).

Recent investigations to suppress VIV stemmed from the original work of Tombazis & Bearman (1997) and Bearman & Owen (1998), where they investigated the influence of an imposed spanwise waviness of the flow separation lines around bluff bodies. They achieved a drag reduction of 30% and a suppression of classical vortex shedding. A principal idea is to weaken vortex shedding without the drag increase associated with traditional "helical strakes" (Zdravkovich 1981). Subsequently, Owen et al. (2001) studied the effects of a sinuous waviness to the axis of a cylinder, as well as the effects of introducing hemispherical bumps to the cylinder surface, which yield an encouraging 25%–47% reduction in drag. These methods diminished the value of mass-damping below which vibrations set in, as shown in Figure 16*b*, but have not completely eliminated the problem of VIV. Introduction of trip wires by Hover et al. (2001) have also diminished the response magnitude and regime of lock-in for VIV.

Finally, we mention the dynamics of tethered structures. In the case of tethered spheres, Govardhan & Williamson (1997, 2003), Williamson & Govardhan (1997), and Jauvtis et al. (2001) explored a wide range of masses, $m^* = 0.1$–1000, and a range of velocities from $U^* = 0$–300, by using both light spheres in a water channel facility and heavy spheres in a wind tunnel. They found a number of modes of response, analogous to the cylinder VIV problem, yielding

amplitudes up to one diameter. The principal vortex structure in Figure 19*a* appears to be a system of streamwise vortex loops (Govardhan & Williamson 2003), which can be related with the vortex force on the body giving rise to vibration. They compiled a Griffin plot for the sphere VIV problem, and also deduced a critical mass, in analogy to the cylinder studies described above. The group of Kerry Hourigan and Mark Thompson at Monash University are conducting studies, both computational and experimental, not only on the tethered sphere problem, but also on the problem of a tethered cylinder (a horizontal cylinder tethered by lever arms to the floor of a water channel). Up to this point, the tethered cylinder results (Ryan et al. 2003) indicate two modes of response, broadly described as an in-line oscillation for small layover angle, corresponding to a classic Karman street wake, and a transverse oscillation for larger tether angles at higher flow speeds, corresponding with the formation of vortex pairs in Figure 19*b*.

10. CONCLUDING REMARKS

In this review, we discuss many of the new fundamental results, but we do not cover all topics fully. Excellent work has been done by many researchers to bring the fundamentals into practical design codes. There is clearly inadequate full-scale data for fluid-structure interactions in a variety of conditions, including sheared flows in the ocean. VIV behavior at large Re is in need of a parallel effort to see which phenomena in this review remain relevant to full-scale structures, and to discover what new phenomena appear. VIV suppression is important. Further understanding of the modes and regimes for yawed cylinders is needed, following Ramberg's (1983) key work. There are ongoing efforts to model, compute, and undertake experiments concerning cable and riser tube dynamics in ocean engineering.

There are some important efforts underway to explore phenomena at high Reynolds numbers. Triantafyllou (2003) has described some high $\mathrm{Re} \sim 10^6$ experiments, taken from a massive facility in St. Johns, Newfoundland, which suggest the existence of distinct response branches and the 2S and 2P modes, although as yet the key results have not been made public. A further significant result has been presented by Bearman et al. (2001), who have presented excellent agreement between in-line response measurements at $\mathrm{Re} \sim 10^4$ (at Imperial College, London) and at $\mathrm{Re} \sim 10^5$ (at the large Delta Flume, Delft, Netherlands). There was also good agreement for the limited transverse VIV response data at these Re. In essence, we have encouraging signs of agreement between laboratory-scale response with full-scale VIV data, but there is no complete comparison for transverse VIV at high Re that is yet available in the public domain. There is a distinct need for further high Re experiments in VIV. One of the most fundamental questions concerning VIV is, what is the maximum attainable amplitude in VIV of an elastically mounted cylinder? We may also ask, what is the functional relationship between

peak amplitudes and mass-damping, in the Griffin plot? Surprisingly, neither of these questions has been answered definitively, although there are ongoing efforts to yield precise well-defined data. On the other hand, owing principally to the two-dimensional computations, we present in this review an accurate determination of the maximum amplitude and definition of the Griffin plot for the laminar regime, at $\mathrm{Re} < 200$.

What generic characteristics exist for VIV, which carry across from the paradigm of the elastically mounted cylinder, in transverse vibration, to more complex systems? It is fascinating that the response branches for this "simple" paradigm are found similarly for cylinders in XY motion, for flexible cantilevers, for pivoted cylinders, for vibrating cables, and possibly for other systems. Analagous modes are found also for tethered bodies. Vortex wake modes that are now known to cause free vibration, at moderate Re, comprise the following set:

$$\{2S, 2P, 2T, 2C\},$$

and in the laminar regime, the set comprises only $\{2S\}$. For VIV systems with spanwise amplitude variation, we observe the 2S-2P Hybrid mode. The P + S mode, ubiquitous in forced vibrations, apparently does not induce free vibration. Conditions where such free-vibration modes exist in these VIV systems correspond well with the Williamson & Roshko (1988) map of modes in the plane of amplitude-velocity, compiled from forced vibration experiments. The concept of a critical mass has been introduced, whereby the regime of synchronization extends to infinite flow velocity—in a sense the body resonates forever! Values of critical mass have been identified for several VIV systems, under conditions of low mass-damping, such as the cylinder in Y-only motion, as well as XY motion, the pivoted cylinder, the tethered sphere, and so on. In fact, one expects to find a critical mass for all VIV systems. In essence, we continue to find generic or universal features that are common to all VIV systems.

Some debates continue on VIV problems, for example the "controversy" regarding added mass, and the problem of relating data from controlled vibrations with the results from free vibration. There is also debate about whether results from our paradigm, the Y-only free vibration of a cylinder, carry across to two degrees of freedom (XY motion). Fortunately, for the hundreds of papers concerned with the paradigm, the results generally carry across very well. However, this similarity breaks down for very low vibrating mass.

Further ideas have been developed in the last few years. One of these ideas is the concept of utilizing vorticity dynamics to measure the force on bodies, which received a boost from the increased capabilities to simulate flows, and to accurately evaluate vorticity using PIV in experiment. Another recent fundamental contribution is the use of the effective elasticity concept to reduce the number of parameters to define the VIV problem for very small damping. As the tools of analysis, simulation, and experiment are further sharpened, we may expect more fundamentally new contributions to emerge, and further universal or generic characteristics to be discovered, which carry across from one VIV system to another.

ACKNOWLEDGMENTS

Immense thanks are due to Nathan N. Jauvtis for extremely enthusiastic and capable help and advice during the preparation of this review. Sincere thanks are also due to G.G. Gupta, C. Cerretelli, M. Horowitz, and B. Ken Davies for their highly valued help. We gratefully acknowledge the support from the Ocean Engineering Division of the Office of Naval Research (O.N.R.), monitored by Dr. Tom Swean (O.N.R. Contract No. N00014–95–1–0332). The support from the O.N.R. for a number of research groups is largely responsible for the existence of the three *BBVIV* International conferences on this topic, for the strong resurgence of interest in this field over the last decade, and indeed for this review on VIV.

LITERATURE CITED

Anagnostopoulos P. 1994. Numerical investigation of response and wake characteristics of a vortex-excited cylinder in a uniform stream. *J. Fluids Struct.* 8:367–90

Anagnostopoulos P. 2000a. Numerical study of the flow past a cylinder excited transversely to the incident stream. Part 1: Lock-in zone, hydrodynamic forces and wake geometry. *J. Fluids Struct.* 14:819–51

Anagnostopoulos P. 2000b. Numerical study of the flow past a cylinder excited transversely to the incident stream. Part 2: Timing of vortex shedding, aperiodic phenomena and wake parameters. *J. Fluids Struct.* 14:853–82

Anagnostopoulos P, ed. 2002. *Flow-Induced Vibrations in Engineering Practice.* Ashurst, UK: WIT Press

Anagnostopoulos P, Bearman PW. 1992. Response charecteristics of a vortex-excited cylinder at low Reynolds numbers. *J. Fluids Struct.* 6:39–50

Anand NM, Torum A. 1985. Free span vibration of submerged pipelines in steady flow and waves. In *Proc. Int. Symp. Separated Flow Around Mar. Struct.*, pp. 155–99. Trondheim, Norway

Angrilli F, Disilvio G, Zanardo A. 1974. Hydroelasticity study of a circular cylinder in a water stream. In *Flow-Induced Structural Vibrations*, ed. E Naudascher, pp. 504–12. Berlin: Springer-Verlag

Aref H, Stremler MA. 1996. On the motion of three-point vortices in a periodic strip. *J. Fluid Mech.* 314:1–25

Balasubramanian S, Skop RA, Haan FL, Szewczyk AA. 2000. Vortex-excited vibrations of uniform pivoted cylinders in uniform and shear flow. *J. Fluids Struct.* 14:65–85

Batchelor GK. 1967. *An Introduction to Fluid Mechanics*. §7.2 New York: Cambridge Univ. Press

Bearman PW. 1984. Vortex shedding from oscillating bluff bodies. *Annu. Rev. Fluid Mech.* 16:195–222

Bearman PW, Johanning L, Owen JC. 2001. Large-scale laboratory experiments on vortex-induced vibration. *Proc. OMAE '01—20th Int. Conf. on Offshore Mech. and Arctic Eng.*, Rio de Janeiro, Brazil, 3–8 June

Bearman PW, Owen JC. 1998. Reproduction of bluff-body drag and suppression of vortex shedding by the introduction of wavy separation lines. *J. Fluids Struct.* 12:123–30

Bearman PW, Williamson CHK. 1998. *Proc. Conf. Bluff Body Wakes and Vortex-Induced Vibrations, Washington, DC*, 21–23 June. Printed at Cornell University, NY. CD-ROM ASME Fluids Eng. Summer Meet., FEDSM98

Bishop RED, Hassan AY. 1964. The lift and drag forces on a circular cylinder oscillating

in a flowing fluid. *Proc. R. Soc. London Ser. A* 277:51–75

Blackburn HM, Govardhan RN, Williamson CHK. 2001. A complementary numerical and physical investigation of vortex-induced vibration. *J. Fluids Struct.* 15:481–88

Blackburn HM, Henderson RD. 1999. A study of two-dimensional flow past an oscillating cylinder. *J. Fluid Mech.* 385:255–86

Blackburn H, Karniadakis GE. 1993. Two and three-dimensional simulations of vortex-induced vibration of a circular cylinder. In *Proc. 3rd Int. Offshore Polar Eng. Conf.* 3: 715–20

Blevins RD. 1990. *Flow-Induced Vibrations*. New York: Van Nostrand Reinhold

Brika D, Laneville A. 1993. Vortex-induced vibrations of a long flexible circular cylinder. *J. Fluid Mech.* 250:481–508

Brika D, Laneville A. 1995. An experimental study of the aeolian vibrations of a flexible circular cylinder at different incidences. *J. Fluids Struct.* 9:371–91

Carberry J, Sheridan J, Rockwell DO. 2001. Forces and wake modes of an oscillating cylinder. *J. Fluids Struct.* 15:523–32

Carberry J, Sheridan J, Rockwell DO. 2003a. Controlled oscillations of a cylinder: a new wake state. *J. Fluids Struct.* 17:337–43

Carberry J, Govardhan R, Sheridan J, Rockwell DO, Williamson CHK. 2003b. Wake states and response branches of forced and freely oscillating cylinder. *Eur. J. Mech. B.* In press

Carberry J, Sheridan J, Rockwell DO. 2003c. Controlled oscillations of a cylinder: forces and wake modes. *J. Fluid Mech.* Submitted

Dean RB, Milligan RW, Wooton LR. 1977. *Study of flow-induced vibration. Atkins Res. Dev. Rep.*, London, UK

Dong P, Benaroya H, Wei T. 2003. Integrating experiments into an energy-based reduced-order model for VIV of a cylinder mounted as an inverted pendulum. *J. Sound Vibr.* In press

Evangelinos C, Karniadakis GE. 1999. Dynamics and flow structures in the turbulent wake of rigid and flexible cylinders subject to vortex-induced vibrations. *J. Fluid Mech.* 400:91–124

Facchinetti ML, DeLangre E, Biolley F. 2002. Vortex shedding modeling using diffusive van der Pol oscillators. *C. R. Méc.* 330:451–56

Facchinetti ML, DeLangre E, Biolley F. 2003. Vortex-induced travelling waves along a cable. *Eur. J. Mech. B.* In press

Feng CC. 1968. *The measurements of vortex-induced effects in flow past a stationary and oscillating circular and D-section cylinders*. Master's thesis. Univ. BC, Vancouver, Can.

Flemming F, Williamson CHK. 2003. Vortex-induced vibrations of a pivoted cylinder. *J. Fluid Mech.* Submitted

Fujarra ALC, Meneghini JR, Pesce CP, Parra PHCC. 1998. An investigation of vortex-induced vibration of a circular cylinder in water. See Bearman & Williamson 1998, Pap. No. 25; Also Pap. FEDSM98-5195, CD-ROM ASME

Fujarra ALC, Pesce CP, Flemming F, Williamson CHK. 2001. Vortex-induced vibration of a flexible cantilever. *J. Fluids Struct.* 15:651–58

Gharib MR, Leonard A, Gharib M, Roshko A. 1998. The absence of lock-in and the role of mass ratio. See Bearman & Williamson 1998, Pap. No. 24; Also Pap. FEDSM98-5312, CD-ROM ASME

Gharib MR, Shiels DG, Gharib M, Leonard A, Roshko A. 1997. Exploration of flow-induced vibration at low mass and damping. *ASME 4th Int. Symp. Fluid-Structure Interaction, Aeroelasticity, Flow-Induced Vibration, and Noise, Dallas, TX*, 16–21 Nov.

Gopalkrishnan R. 1993. *Vortex-induced forces on oscillating bluff cylinders.* PhD thesis. MIT, Cambridge, MA

Govardhan R, Williamson CHK. 1997. Vortex induced motions of a tethered sphere. *J. Wind Eng. Ind. Aerodyn.* 69–71:375–85

Govardhan R, Williamson CHK. 2000. Modes of vortex formation and frequency response for a freely-vibrating cylinder. *J. Fluid Mech.* 420:85–130

Govardhan R, Williamson CHK. 2001. Mean and fluctuating velocity fields in the wake of a freely-vibrating cylinder. *J. Fluids Struct.* 15:489–502

Govardhan R, Williamson CHK. 2002. Resonance forever: existence of a critical mass and an infinite regime of resonance in vortex-induced vibration. *J. Fluid Mech.* 473:147–66

Govardhan R, Williamson CHK. 2003. Vortex-induced vibration of an elastically-mounted sphere. *J. Fluid Mech.* Submitted

Griffin OM. 1980. Vortex-excited cross-flow vibrations of a single cylindrical tube. *ASME J. Pressure Vessel Technol.* 102:158–66

Griffin OM, Ramberg SE. 1974. The vortex street wakes of vibrating cylinders. *J. Fluid Mech.* 66:553–76

Griffin OM, Ramberg SE. 1976. Vortex shedding from a cylinder vibrating in line with an incident uniform flow. *J. Fluid Mech.* 75:257–71

Griffin OM, Ramberg SE. 1982. Some recent studies of vortex shedding with application to marine tubulars and risers. *Trans. ASME J. Energy Resour. Technol.* 104:2–13

Griffin OM, Skop RA, Ramberg SE. 1975. The resonant vortex-excited vibrations of structures and cable systems. In *7th Offshore Technol. Conf., Houston, TX, OTC Pap. 2319*

Gu W, Chyu C, Rockwell D. 1994. Timing of vortex formation from an oscillating cylinder. *Phys. Fluids* 6:3677–82

Guilmineau E, Queutey P. 2000. A numerical simulation of the response of a vortex-excited cylinder. In *Flow Induced Vibration*, ed. S Ziada, T Staubli, pp. 257–64. Rotterdam, Netherlands: Balkema

Guilmineau E, Queutey P. 2002. A numerical simulation of vortex shedding from an oscillating circular cylinder. *J. Fluids Struct.* 16:773–94

Hover F, Davis JT, Triantafyllou MS. 2003. Three-dimensionality of mode transition in vortex-induced vibrations of a circular cylinder. *Eur. J. Mech. B.* In press

Hover F, Davis JT, Triantafyllou MS. 1997. Vortex-induced vibration of marine cables: experiments using force feedback. *J. Fluids Struct.* 11:307–26

Hover FS, Techet AH, Triantafyllou MS. 1998. Forces on oscillating uniform and tapered cylinders in crossflow. *J. Fluid Mech.* 363:97–114

Hover FS, Tvedt H, Triantafyllou MS. 2001. Vortex-induced vibrations of a cylinder with tripping wires. *J. Fluid Mech.* 448:175–95

Iwan WD, Jones NP. 1987. On the vortex-induced oscillation of long structural elements. *Trans. ASME: J. Energy Resour. Technol.* 109:161–67

Jauvtis N, Govardhan R, Williamson CHK. 2001. Multiple modes of vortex-induced vibration of a sphere. *J. Fluids Struct.* 15:555–564

Jauvtis N, Williamson CHK. 2003a. Vortex-induced vibration of a cylinder with two degrees of freedom. *J. Fluids Struct.* 17:1035–42

Jauvtis N, Williamson CHK. 2003b. A high-amplitude 2T mode of vortex formation, and the effects of non-harmonic forcing in vortex-induced vibration. *Eur. J. Mech. B.* In press

Jauvtis N, Williamson CHK. 2003c. The effects of two degrees of freedom on vortex-induced vibration. *J. Fluid Mech.* Submitted

Jeon D, Gharib M. 2001. On circular cylinders undergoing two-degree-of-freedom forced motions. *J. Fluids Struct.* 15:533–41

Khalak A, Williamson CHK. 1996. Dynamics of a hydroelastic cylinder with very low mass and damping. *J. Fluids Struct.* 10:455–72

Khalak A, Williamson CHK. 1997a. Fluid forces and dynamics of a hydroelastic structure with very low mass and damping. *J. Fluids Struct.* 11:973–82

Khalak A, Williamson CHK. 1997b. Investigation of the relative effects of mass and damping in vortex-induced vibration of a circular cylinder. *J. Wind Eng. Ind. Aerodyn.* 69–71: 341–50

Khalak A, Williamson CHK. 1999. Motions, forces and mode transitions in vortex-induced vibrations at low mass-damping. *J. Fluids Struct.* 13:813–51

Kim WJ, Perkins NC. 2002. Two-dimensional vortex induced vibration of cable suspensions. *J. Fluids Struct.* 16:229–45

King R. 1974. Vortex-excited oscillations of a circular cylinder in steady currents. *Offshore Technol. Conf. Pap. OTC 1948*

Koumoutsakos P, Leonard A. 1995. High-resolution simulations of the flow around an impulsively started cylinder using vortex methods. *J. Fluid Mech.* 296:1–38

Krishnamoorthy S, Price SJ, Paidoussis MP. 2001. Cross-flow past an oscillating circular cylinder: Synchronization phenomena in the near wake. *J. Fluids Struct.* 15:955–80

Lamb H. 1932. *Hydrodynamics*. §152 New York: Dover

Leonard A, Roshko A. 2001. Aspects of flow-induced vibration. *J. Fluids Struct.* 15:415–25

Leweke T, Bearman PW, Williamson CHK, eds. 2001. Special Issue on *Bluff Body Wakes and Vortex-Induced Vibrations*. *J. Fluids Struct.* 15:1–669

Leyva J, Rockwell DO, Jauvtis N, Williamson CHK. 2003. A comparative study of XY vortex-induced vibration of a circular cylinder. *J. Fluids Struct.* In preparation

Lighthill J. 1979. Waves and hydrodynamic loading. In *Proc. 2nd Int. Conf. Behav. Off-Shore Struct.* 1:1–40. BHRA Fluid Eng., Cranfield, England

Lighthill J. 1986. Fundamentals concerning wave loading on offshore structures. *J. Fluid Mech.* 173:667–81

Lin JC, Rockwell D. 1996. Force identification by vorticity fields: Techniques based on flow imaging. *J. Fluids Struct.* 10:663–68

Lu XY, Dalton C. 1996. Calculation on the timing of vortex formation from an oscillating cylinder. *J. Fluids Struct.* 10:527–41

Lucor D, Imas L, Karniadakis GE. 2001. Vortex dislocations and force distribution of long flexible cylinders subjected to sheared flows. *J. Fluids Struct.* 15:651–58

Marcollo H, Hinwood JB. 2002. Vortex-induced vibration of a long flexible cylinder in uniform flow with both forcing and response. In *Proc. BBVIV-3 Bluff Body Wakes and Vortex-Induced Vibrations*, ed. K Hourigan, T Leweke, MC Thompson, CHK Williamson, pp. 219–23. Port Douglas, Australia, 17–20 Dec.

Maull DJ, Milliner MC. 1978. Sinusoidal flow past a circular cylinder. *Coast. Eng.* 2:149–68

Meier-Windhorst A. 1939. Flatterschwingungen von Zylindern im gleichmassigen Flussigkeitsstrom. *Mitt. Hydraul. Inst. Tech. Hochsch., Münch.* 9:3–39

Meneghini JR, Bearman PW. 1993. Numerical simulation of high amplitude oscillatory-flow about a circular cylinder using a discrete vortex method. In *Shear Flow Conf. AIAA Pap. 93-3288, Orlando, FL*, Jul. 6–9

Meneghini JR, Bearman PW. 1995. Numerical simulation of high amplitude oscillatory flow about a circular cylinder. *J. Fluids Struct.* 9:435–55

Mercier JA. 1973. *Large amplitude oscillations of a circular cylinder in a low speed stream.* PhD thesis. Stevens Inst. Technol., Hoboken, NJ

Moe G, Overvik T. 1982. Current-induced motions of multiple risers. In *Proc. BOSS-82, Behaviour of Offshore Struct.*, ed. C Chryyostomides, JJ Connor, pp. 618–39. Washington, D.C.: Hemisphere

Moe G, Wu ZJ. 1990. The lift force on a cylinder vibrating in a current. *ASME J. Offshore Mech. Arctic Eng.* 112:297–303

Moreau JJ. 1953. Bilan dynamique d'un ecoulement rotationnel. *J. Math. Pures Appl.* 31: 355–75; 32:1–78

Naudascher E. 1987. Flow-induced streamwise vibrations of structures. *J. Fluids Struct.* 1:265–98

Naudascher E, Rockwell D. 1994. *Flow-Induced Vibrations: An Engineering Guide*. Rotterdam, Netherlands: Balkema

Newman DJ, Karniadakis GE. 1995. Direct numerical simulations of flow over a flexible cable. In *Proc. 6th Int. Conf. Flow-Induced Vibrations*, ed. PW Bearman, pp. 193–203. Rotterdam, Netherlands: Balkema

Newman DJ, Karniadakis GE. 1996. Simulations of flow over a flexible cable:

Comparison of forced and flow-induced vibration. *J. Fluids Struct.* 10:439–53

Newman DJ, Karniadakis GE. 1997. Simulations of flow past a freely vibrating cable. *J. Fluid Mech.* 344:95–136

Noca F, Shiels D, Jeon D. 1997. Measuring instantaneous fluid dynamic forces on bodies, using only velocity fields and their derivatives. *J. Fluids Struct.* 11:345–50

Noca F, Shiels D, Jeon D. 1999. A comparison of methods for evaluating time-dependent fluid dynamic forces on bodies, using only velocity fields and their derivatives. *J. Fluids Struct.* 13:551–78

Ongoren A, Rockwell D. 1988a. Flow structure from an oscillating cylinder. Part 1. Mechanisms of phase shift and recovery in the near wake. *J. Fluid Mech.* 191:197–223

Ongoren A, Rockwell D. 1988b. Flow structure from an oscillating cylinder. Part 2. Mode competition in the near wake. *J. Fluid Mech.* 191:225–45

Owen JC, Bearman PW, Szewczyk AA. 2001. Passive control of VIV with drag reduction. *J. Fluids Struct.* 15:597–606

Parkinson GV. 1974. Mathematical models of flow induced vibrations of bluff bodies. In *Flow-Induced Structural Vibrations*, ed. E Naudascher, pp. 81–127. Berlin: Springer-Verlag

Parkinson GV. 1989. Phenomena and modelling of flow-induced vibrations of bluff bodies. *Prog. Aerosp. Sci.* 26:169–224

Pesce CP, Fujarra ALC. 2000. Vortex-induced vibrations and jump phenomenon: experiments with a clamped flexible cylinder in water. *Int. J. Offshore Polar Eng.* 10:26–33

Porta FL, Aref H. 2003. Numerical experiments on vortex shedding from an oscillating cylinder. *J. Fluid Mech.* Submitted

Ramberg SE. 1983. The effects of yaw and finite length upon the vortex wakes of stationary and vibrating circular cylinders. *J. Fluid Mech.* 128:81–107

Roshko A, Leonard A, Shiels D. 2000. Flow induced vibration of a circular cylinder: A unified description. In *Abstracts for IUTAM Symp. Bluff Body Wakes Vortex-Induced Vibrations BBVIV-2*, ed. PW Bearman, T Leweke, CHK Williamson, Abstract #1. Marseille, France, 13–16 June

Ryan K, Carberry J, Sheridan J, Thompson MC, Hourigan K. 2003. Two states of oscillation for a buoyant tethered cylinder. *J. Fluids Struct.* Submitted

Saffman PG. 1992. *Vortex Dynamics*. Cambridge Univ. Press

Saltara F, Meneghini JR, Siqueira CR, Bearman PW. 1998. The simulation of vortex shedding from an oscillating circular cylinder with turbulence modelling. See Bearman & Williamson 1998, Pap. No. 25; Also Pap. FEDSM98-5189, CD-ROM ASME

Sarpkaya T. 1977. Transverse oscillations of a circular cylinder in uniform flow, Part 1. *Rep. No. NPS-69SL77071, Nav. Postgrad. Sch.*, Monterey, CA

Sarpkaya T. 1978. Fluid forces on oscillating cylinders. *ASCE J. Waterway Port Coast. Ocean Div.* 104:275–90

Sarpkaya T. 1979. Vortex-induced oscillations. *ASME J. Appl. Mech.* 46:241–58

Sarpkaya T. 1993. Offshore hydrodynamics. *ASME J. Offshore Mech. Arctic Eng.* 115: 2–5

Sarpkaya T. 1995. Hydrodynamic damping, flow-induced oscillations, and biharmonic response. *ASME J. Offshore Mech. Arctic Eng.* 117:232–38

Sarpkaya T. 2001. On the force decompositions of Lighthill and Morison. *J. Fluids Struct.* 15:227–33

Scruton C. 1965. On the wind-excited oscillations of towers, stacks and masts. In *Proc. Symp. Wind Effects Build. Struct.*, Pap. 16, pp. 798–836. London: HMSO

Sheridan J, Carberry J, Lin JC, Rockwell D. 1998. On the near wake topology of an oscillating cylinder. *J. Fluids Struct.* 12:215–20

Shiels D, Leonard A, Roshko A. 2001. Flow-induced vibration of a circular cylinder at limiting structural parameters. *J. Fluids Struct.* 15:3–21

Skop RA. 1974. On modelling vortex-excited oscillations. *NRL Memo. Rep. 2927*

Skop RA, Balasubramanian S. 1997. A new twist on an old model for vortex-excited vibrations. *J. Fluids Struct.* 11:395–412

Skop RA, Griffin OM. 1973. An heuristic model for determining flow-induced vibrations of offshore structures. In *5th Offshore Technology Conf., OTC Pap. 1843.* Houston, TX

Skop RA, Luo G. 2001. An inverse-direct method for predicting the vortex-induced vibrations of cylinders in uniform and nonuniform flows. *J. Fluids Struct.* 15:867–84

Stansby PK. 1976. The locking-on of vortex shedding due to the cross-stream vibration of circular cylinders in uniform and shear flows. *J. Fluid Mech.* 74:641–55

Staubli T. 1983. Calculation of the vibration of an elastically-mounted cylinder using experimental data from forced oscillation. *ASME J. Fluids Eng.* 105:225–29

Stokes GG. 1851. On the effect of the internal friction of fluids on the motion of pendulums. *Trans. Cambridge Philos. Soc.* 9:8–106

Sumer BM, Fredsøe J. 1997. *Hydrodynamics around Cylindrical Structures.* Singapore: World Sci.

Techet AH, Hover FS, Triantafyllou MS. 1998. Vortical patterns behind a tapered cylinder oscillating transversely to a uniform flow. *J. Fluid Mech.* 363:79–96

Tombazis N, Bearman PW. 1997. A study of three-dimensional aspects of vortex shedding from a bluff body with a mild geometric disturbance. *J. Fluid Mech.* 330:85–112

Triantafyllou MS, Hover FS, Yue DKP. 2003. Vortex-induced vibrations of slender structures in shear flow: A review. In *IUTAM Symp. Coupled Fluid-Structure Interaction using Analysis, Computations and Experiments*, ed. H Benaroya, T Wei, Paper I-6. Rutgers, NJ

Triantafyllou MS, Grosenbaugh MA. 1995. Prediction of vortex-induced vibrations in sheared flows. In *Flow-Induced Vibration*, ed. PW Bearman, pp. 73–82. Rotterdam, Netherlands: Balkema

Unal MF, Lin JC, Rockwell D. 1997. Forced prediction by PIV imaging: A momentum-based approach. *J. Fluids Struct.* 11:965–71

Vandiver JK. 1993. Dimensionless parameters important to the prediction of vortex-induced vibration of long flexible cylinders in ocean currents. *J. Fluids Struct.* 7:423–55

Vandiver JK. 2003. SHEAR 7 User Guide. Dept. Ocean Eng., MIT

Vandiver JK, Jong J-Y. 1987. The relationship between in-line and cross-flow vortex-induced vibration of cylinders. *J. Fluids Struct.* 1:381–99

Vandiver JK, Marcollo H. 2003. High mode number VIV experiments. In *IUTAM Fully Coupled Fluid-Structure Interaction*, ed. H Benaroya, T Wei, Netherlands: Kluwer. In press

Vickery BJ, Watkins RD. 1964. Flow-induced vibrations of cylindrical structures. In *Proc. 1st Aust. Conf. Hydraul. Fluid Mech.*, ed. R Silvester, pp. 213–41. New York: Pergamon

Vikestad K, Vandiver JK, Larsen CM. 2000. Added mass and oscillation frequency for a circular cylinder subjected to vortex-induced vibrations and external disturbance. *J. Fluids Struct.* 14:1071–88

Voorhees A, Wei T. 2002. Three-dimensionality in the wake of a surface piercing cylinder mounted as an inverted pendulum. In *Proc. BBVIV-3 Bluff Body Wakes and Vortex-Induced Vibrations*, ed. K Hourigan, T Leweke, MC Thompson, CHK Williamson, pp. 133–36. Port Douglas, Australia, 17–20 Dec.

Weiss LG, Szewczyk AA. 2000. An experimental investigation of some three-dimensional effects of pivoted circular cylinders. In Flow Induced Vibration, ed. S Ziada, T Staubli, p. 75–83. Rotterdam, Netherlands: Balkema

Willden RHJ, Graham JMR. 2001. Numerical prediction of VIV on long flexible circular cylinders. *J. Fluids Struct.* 15:659–69

Williamson CHK. 1985. Sinusoidal flow relative to circular cylinders. *J. Fluid Mech.* 155:141–74

Williamson CHK. 1992. The natural and forced formation of spot-like L-structures caused

by vortex dislocations in wake transition. *J. Fluid Mech.* 243:393–441

Williamson CHK, Govardhan R. 1997. Dynamics and forcing of a tethered body in a fluid flow. *J. Fluids Struct.* 11:293–305

Williamson CHK, Roshko A. 1988. Vortex formation in the wake of an oscillating cylinder. *J. Fluids Struct.* 2:355–81

Wooton LR, Warner MH, Sainsbury RN, Cooper DH. 1972. Oscillations of piles in marine structures. A resume of full-scale experiments at Immingham. *CIRIA Tech. Rep. 41*

Zdera R, Turan ÖF, Havard DG. 1995. Towards understanding galloping: Near-wake study of oscillating smooth and stranded circular cylinders in forced motion. *Exp. Therm. Fluid Sci.* 10:28–43

Zdravkovich MM. 1981. Review and classification of various aerodynamic and hydrodynamic means for supressing vortex shedding. *J. Wind Eng. Ind. Aerodyn.* 7:145–89

Zdravkovich MM. 1982. Modification of vortex shedding in the synchronization range. *ASME J. Fluids Eng.* 104:513–17

Zdravkovich MM. 1990. On origins of hysteretic responses of a circular cylinder induced by vortex shedding. *Z. Flugwiss. Weltraumforsch.* 14:47–58

Zhou CY, So RMC, Lam K. 1999. Vortex-induced vibrations of an elastic circular cylinder. *J. Fluids Struct.* 13:165–89

APPENDIX Nondimensional Groups

Mass ratio	m^*	$\frac{m}{\pi\rho D^2 L/4}$
Damping ratio	ζ	$\frac{c}{2\sqrt{k(m+m_A)}}$
Velocity ratio	U^*	$\frac{U}{f_N D}$
Amplitude ratio	A^*	$\frac{y_o}{D}$
Frequency ratio	A^*	$\frac{f}{f_N}$
Streamwise force coefficient	C_X	$\frac{F_X}{\frac{1}{2}\rho U^2 DL}$
Transverse force coefficient	C_Y	$\frac{F_Y}{\frac{1}{2}\rho U^2 DL}$
Reynolds number	Re	$\frac{\rho U D}{\mu}$

Notes regarding these groups:

- We use f_N as the natural frequency in still water, and correspondingly use ζ as the ratio of (structural damping)/(critical damping in water). The frequency f, used in f^*, is the actual body oscillation frequency during induced vibration.
- The added mass, $m_A = C_A m_d$, where $m_d = \pi\rho D^2 L/4$ is the displaced mass of fluid, and where L is the cylinder length, and $c_A = 1.0$.

NOTE ADDED IN PROOF

Ponta & Aref (2003) found similar vortex dynamics in their simulations of the laminar regime ($Re = 140$). An interesting contribution of their work is the suggestion that the mode boundaries in the Williamson and Roshko map are related to the deviation of the instantaneous vortex shedding period relative to its value at the peak Reynolds number found in a cycle. This brings in a dependence on Reynolds number and thus might be related to the existence of the 2P mode at turbulent Re ($Re > 200$), and its replacement by the P + S mode in the laminar regime ($Re < 200$). They also suggest the possible existence of other "exotic" wake modes based on results from their point vortex models (Aref & Stremler 1996, and other ongoing studies).

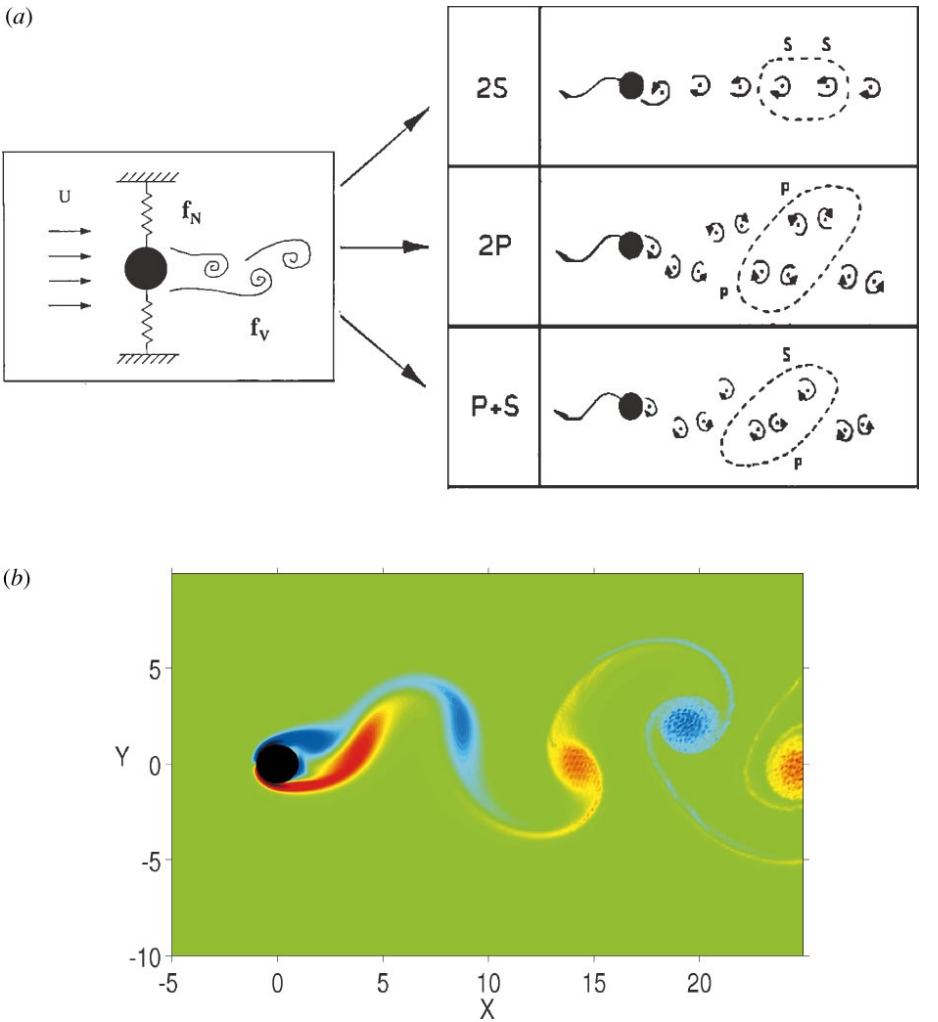

Figure 1 (*a*) Schematic diagram of an elastically mounted cylinder, restrained to vibrate transverse to the free stream (Y-direction). A feedback between the fluid and body motion is now known to lead to several different vortex formation modes, for example, the 2S mode (comprising two single vortices per cycle of motion) or the 2P mode (comprising two vortex pairs per cycle). The P + S mode, ubiquitous in low-Re forced vibration, is never found in free vibration. (*b*) The wake and vortex-induced vibrations of a cylinder, which has no mass, no damping, and no springs, and so is disconnected from mechanical structure in the transverse direction. Shiels et al. (2001) discovered, from numerical simulation at Re = 100, that the body undergoes large-amplitude vibration at a frequency close to the fixed-body vortex shedding frequency.

(a)

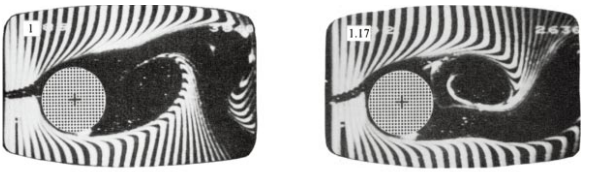

(b)

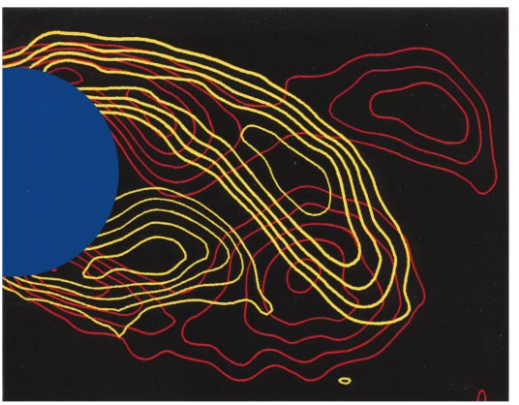

(c)

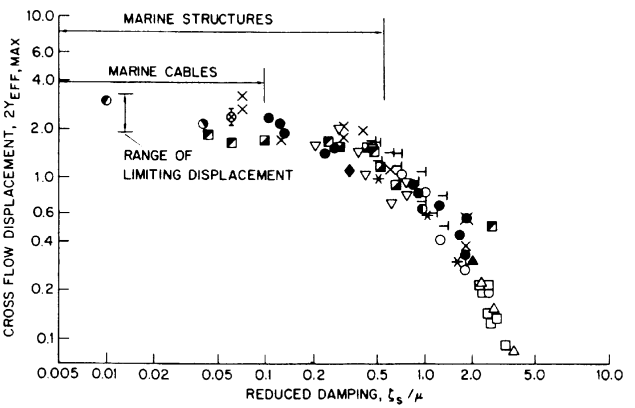

(d)

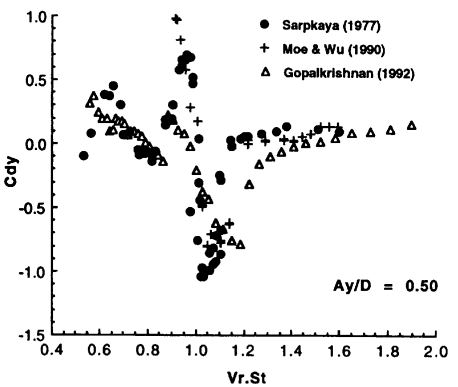

See legend on next page

Figure 3 Some classic results from vortex-induced vibration (VIV). (*a*) shows the switch in timing of vortex shedding as forced vibration frequency increases (Ongoren & Rockwell 1988a). (*b*) presents the same phenomenon using the Particle Image Velocimetry technique, and represents the first use of this technique in the VIV field (Gu, Chyu & Rockwell 1994). Yellow vorticity magnitude contours are for low frequency, with the body at the top of its vertical motion. Red contours are for higher frequencies above a critical value for the switch in timing, again for the body at the top of its motion. (*c*) presents one of the original Griffin plots, showing peak amplitudes plotted versus the Skop-Griffin parameter (S_G), from Griffin (1980). (*d*) shows the agreement of force coefficient (C_{DY}) data from Moe & Wu (1990) and Gopalkrishnan (1993), with Sarpkaya's (1977) well-known data. Taken from Sarpkaya (1995).

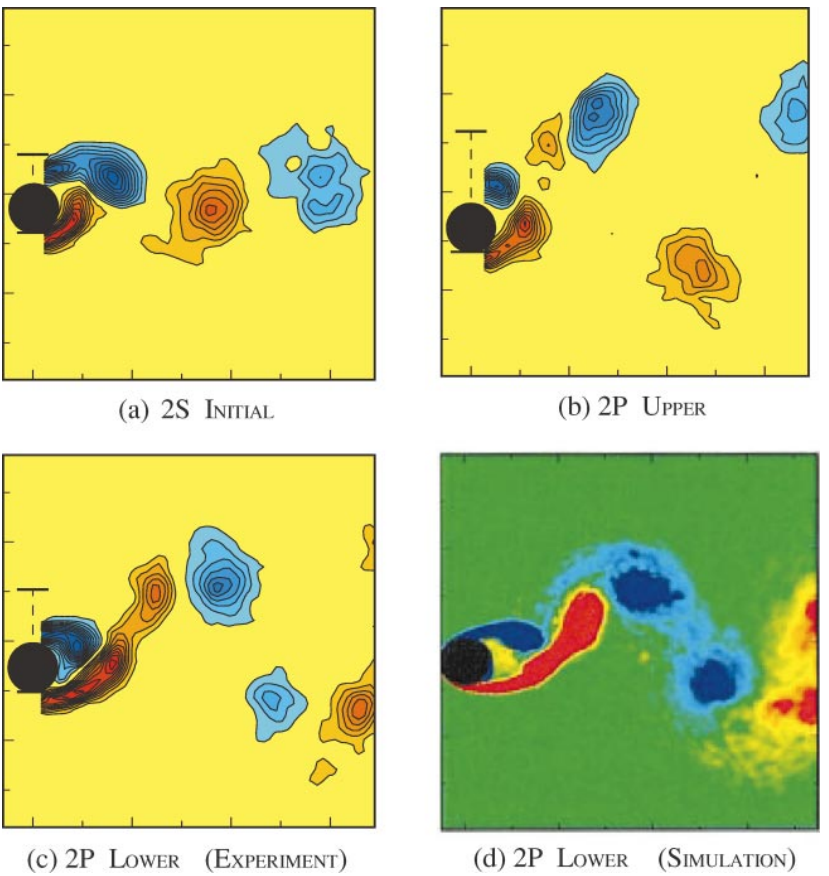

Figure 6 Evidence from Particle-Image Velocimetry vorticity measurements in free vibration that the initial branch corresponds with the 2S vortex wake mode, and that the upper and lower branches both reflect the 2P mode (Govardhan & Williamson 2000). Blackburn et al. (2001) make a good comparison, computing the 2P mode of the lower branch, which is only possible with 3D simulations.

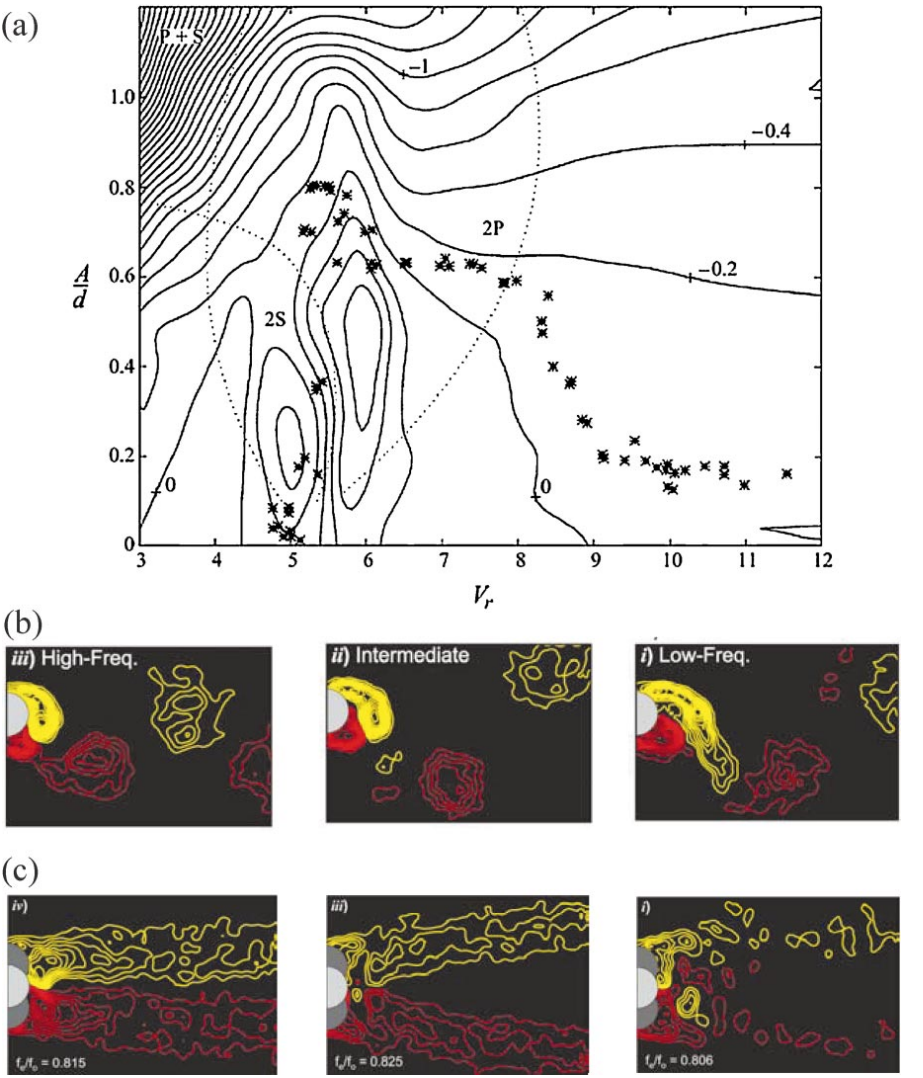

Figure 11 Contours of excitation ($C_Y \sin \phi$), in (*a*), from Hover et al. (1998), compare well with free-vibration response amplitudes, evaluated from their ingenious force-feedback virtual cable testing apparatus. V_r is the true reduced velocity, equivalent to (U*/f*). Forced vibrations in (*b*) show the 2S-2P-2P modes corresponding with the high-intermediate-low frequency modes of Carberry et al. (2003b). Mean vorticity contours are shown in (*c*) corresponding to the same modes in (*b*).

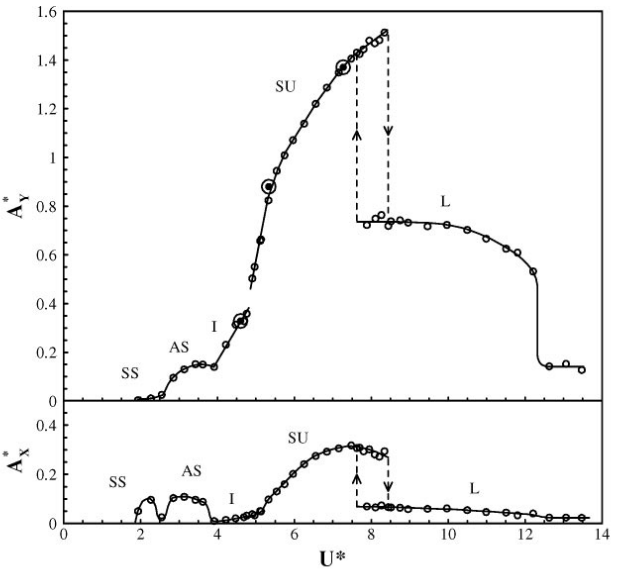

(a) XY – Motion response amplitudes.

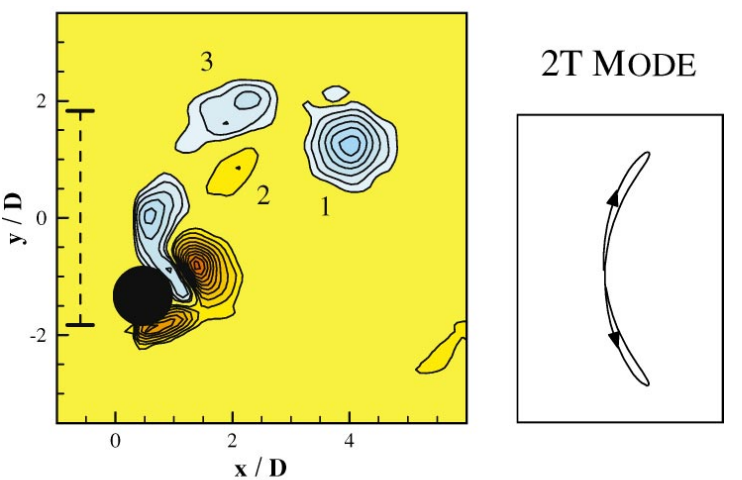

(b) 2T Mode of vortex formation.

Figure 15 Discovery of a "super-upper" branch of high-amplitude response that appears for XY cylinder vibration when mass ratios, $m^* < 6$. This corresponds with the appearance of a "2T" vortex wake mode, comprising a triplet of vortices to form in each half cycle. From Jauvtis & Williamson (2003b,c).

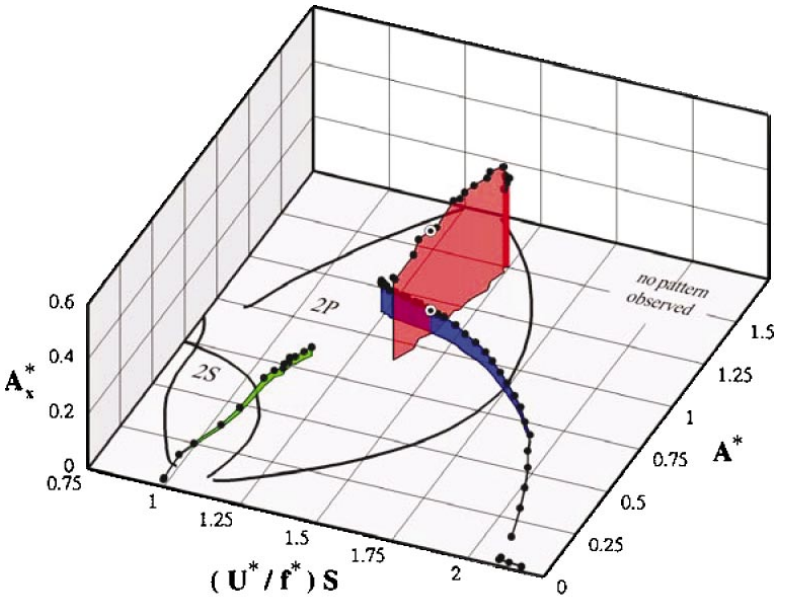

(a) 3-D response plot for a pivoted cylinder.

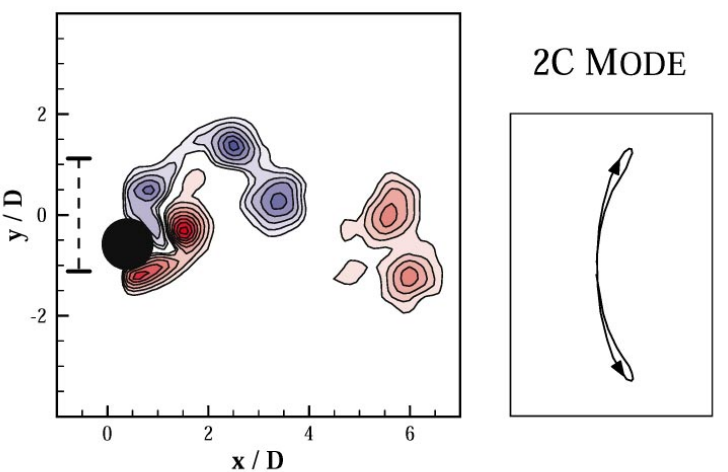

(b) 2C Mode of vortex formation.

Figure 17 Response amplitude branches for a pivoted cylinder, exhibited in a three-dimensional version of the Williamson & Roshko (1988) map of modes, and the corresponding "2C" vortex mode (*below*), comprising two corotating vortices each half cycle, which appears for the high-amplitude branch. From Flemming & Williamson (2003).

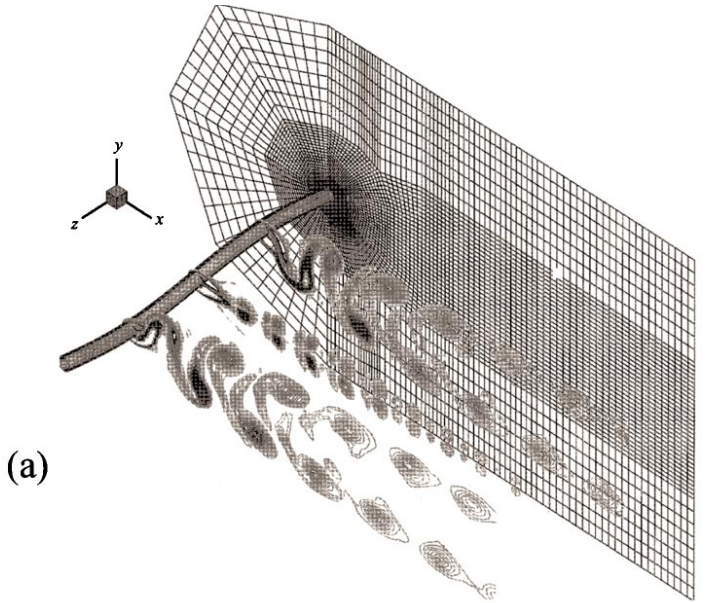

(a)

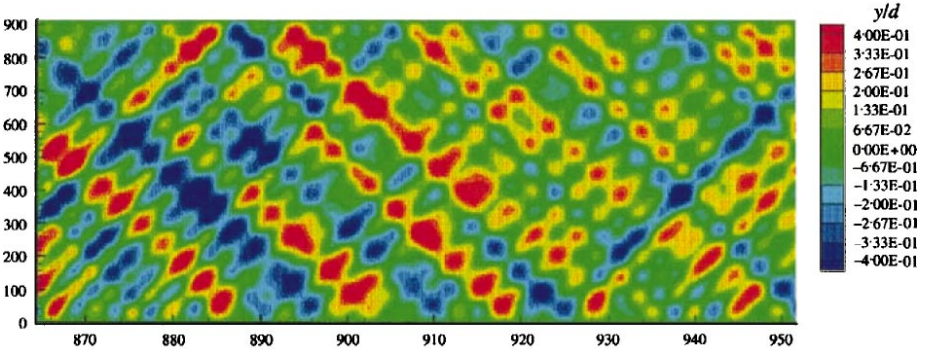

(b)

Figure 18 Three-dimensional computations of vortex-induced vibration of a flexible cable are now possible; here we see wake vortex dynamics at nodes and antinodes of a cable vibrating with a standing wave (Newman & Karniadakis 1996, 1997). Further results from the research group at Brown University show contours of transverse amplitude along the span of a cable (*vertical axis*) as a function of time (*horizontal axis*), for a cable undergoing a mixed response of traveling and standing waves.

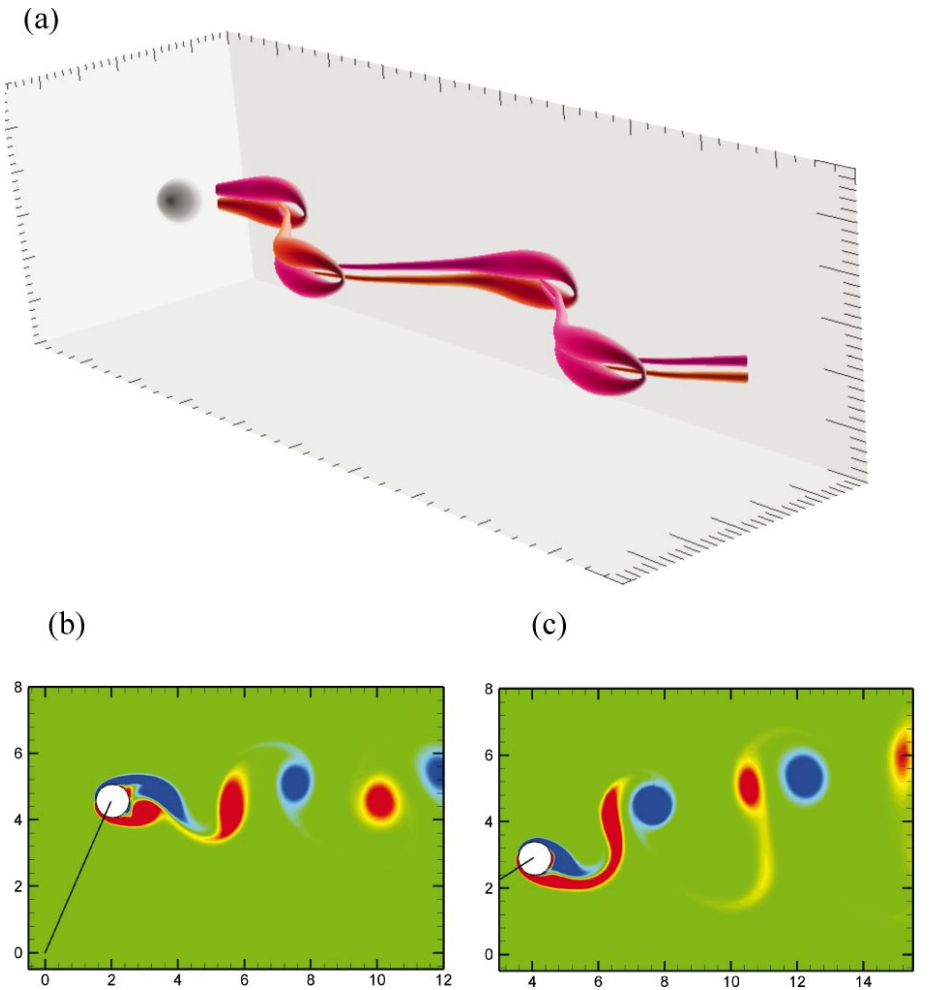

Figure 19 Dynamics of tethered bodies. In (*a*), one of the principal modes of tethered sphere oscillation comprises a periodic streamwise vortex loop wake, which gives rise to transverse forces necessary to sustain free vibration (Govardhan & Williamson 2003). In (*b*) and (*c*), one finds two distinct modes of vibration for a tethered cylinder (Ryan et al. 2003). A low-amplitude mode at low velocities gives rise to a classical vortex street (*b*), with a tether angle of 27°. In (*c*), an increased flow velocity leads to a higher-amplitude mode involving a vortex-pairing wake, for a tether angle of 44°.

Annual Review of Fluid Mechanics
Volume 36, 2004

CONTENTS